Acta Mech 230, 1077–1103 (2019)
https://doi.org/10.1007/s00707-018-2334-9

ORIGINAL PAPER

Saeid Sahmani · Mohamad Fotouhi · Mohammad Mohammadi Aghdam

Size-dependent nonlinear secondary resonance of micro-/nano-beams made of nano-porous biomaterials including truncated cube cells

Received: 14 February 2018 / Revised: 22 October 2018 / Published online: 27 December 2018

Abstract Porous biomaterials have been utilized in cellular structures in order to mimic the function of bone as a branch of tissue engineering approach. With the aid of nano-porous biomaterials in which the pore size is at nanoscale, the capability of biological molecular isolation becomes more efficient. In the present study, first the mechanical properties of nano-porous biomaterials are estimated on the basis of a truncated cube cell model including a refined hyperbolic shear deformation for the associated lattice structure. After that, based upon a nonlocal strain gradient beam model, the size-dependent nonlinear secondary resonance of micro-/nano-beams made of the nano-porous biomaterial is predicted corresponding to both subharmonic and superharmonic excitations. The nonclassical governing differential equation of motion is constructed via Hamilton's principle. By employing the Galerkin technique together with the multiple-timescale method, the nonlocal strain gradient frequency response and amplitude response of the nonlinear oscillation of micro-/nano-beams made of a nano-porous biomaterial under hard excitation are achieved. It is shown that in the superharmonic case, increasing the pore size leads to an enhancement of the nonlinear hardening spring-type behavior of the jump phenomenon and the height of limit point bifurcations. In the subharmonic case, higher pore size causes an increase in the gap between two branches associated with the high-frequency and low-frequency solutions.

1 Introduction

Biomaterials have the capability to be used in structures replacing a part or a function of a living organism in a reliable way without adversely affecting it. In order to display tissue formation more efficiently, porous biomaterials are utilized which allow proliferation and vascularization of a living cell as well as interlocking between the biomaterial and surrounding natural tissue.

By rapid advancements in science and technology, more effective methods to deliver and release drugs into the body have been determined. Using porous nano-structures is one of these efficient ways for controlling the delivery of a drug [1–3]. Having a high surface area with several pores makes porous nano-structures an ideal candidate for the encapsulation of pharmaceutical drugs [4]. Also, vibration analysis is an important study in

S. Sahmani (✉)
Mechanical Rotating Equipment Department, Niroo Research Institute (NRI), Tehran 16656-517, Iran
E-mail: sahmani@aut.ac.ir
Tel.: +98 21 66405844
Fax: +98 21 66419736

M. Fotouhi
Design and Mathematics Department, University of the West England, Bristol BS16 1QY, UK

M. M. Aghdam
Mechanical Engineering Department, Amirkabir University of Technology, Tehran 15875-4413, Iran

biomedical applications. For instance, Usui et al. [5] investigated radiographically and biomechanically the effects of mechanical vibration on bone ingrowth into porous hydroxyapatite implants and fracture healing in a rabbit model. Altintas [6] performed a modal vibration analysis of a heterogeneous porous structure by taking microstructural details into consideration.

Through miniaturizing a solid material to nanoscale, size dependency characteristics take on an importance which are normally inconsequential at usual scale. This size-induced property change has inspired the development of several size-dependent continuum theories such as nonlocal elasticity theory [7], surface elasticity theory [8], strain gradient elasticity theory [9] and couple stress elasticity theory [10]. In recent years, a variety of studies has been conducted to employ these nonclassical continuum theories of elasticity to investigate crucial characteristics of the mechanical response of nano-structures [11–50].

Recently, Lim et al. [51] have introduced a refined nonlocal continuum mechanics, namely the nonlocal strain gradient elasticity theory, including simultaneously both hardening stiffness and softening stiffness of the size effect. After that, some studies have been carried out to construct the integral elasticity type of this theory [52,53]. In recent years, the newly proposed elasticity theory has been widely utilized to capture stress and strain gradient scaling effects on the mechanical behavior of micro-/nano-structures. Tang et al. [54] developed a nonlocal strain gradient Timoshenko beam model for wave dispersion in a viscoelastic single-walled carbon nanotube. Li et al. [55] analyzed bending, buckling and vibration of axially functionally graded nano-beams on the basis of the nonlocal strain gradient elasticity theory. Ebrahimi and Dabbagh [56] predicted the flexural wave propagation of functionally graded magneto-electro-elastic nano-plates based upon the nonlocal strain gradient theory of elasticity. Sahmani and Aghdam [57] employed the nonlocal strain gradient elasticity theory to analyze the nonlinear instability of axially loaded microtubules surrounded by the cytoplasm of a living cell. Lu et al. [58] explored the size-dependent free vibrations of nano-beams by incorporating the nonlocal strain gradient theory into the sinusoidal shear deformation beam theory. Sahmani and Aghdam [59] constructed a nonlocal strain gradient shell model to anticipate buckling and postbuckling behavior of axially loaded multilayer functionally graded nano-shells reinforced with graphene platelets. Zhu and Li [60] proposed a closed-form solution based upon nonlocal strain gradient elasticity theory for a small-scaled rod in tension. Sahmani and Aghdam [61] used the nonlocal strain gradient continuum mechanics to examine the nonlinear instability of hydrostatic pressurized multilayer functionally graded nano-shells reinforced with graphene nano-platelets. Li and Hu [62] investigated the size-dependent postbuckling behavior of functionally graded nano-beams including nonlocality and strain gradient size dependency. Sahmani and Aghdam [63] constructed a nonlocal strain gradient higher-order shear deformable beam model for nonlinear vibration analysis of postbuckling multilayer functionally graded nano-beams. They also predicted the nonlinear primary resonance of a nano-beam made of nano-porous biomaterial subjected to soft excitation [64]. Radwan and Sobhy [65] developed a nonlocal strain gradient plate model for dynamic deformation of viscoelastic graphene nano-sheets under harmonic thermal load. Sahmani et al. [66–68] analyzed the size-dependent nonlinear mechanical behaviors of reinforced functionally graded porous micro-/nano-structures on the basis of the nonlocal strain gradient theory of elasticity. Recently, Li et al. [69] have investigated the influence of the beam thickness on the size-dependent buckling and postbuckling characteristics of nano-beams modeled via the nonlocal strain gradient theory.

The objective of this work is to predict the size-dependent nonlinear secondary resonance of a micro-/nano-beam made of nano-porous biomaterials including truncated cubic unit cells. To accomplish this, the mechanical properties of the nano-porous biomaterial comprising the truncated cube cells including a refined hyperbolic shear deformation effect are obtained as analytical functions of the pore size. After that, based on the nonlocal strain gradient elasticity theory, a size-dependent beam model is constructed. By using the Galerkin technique together with the multiple-timescale method, analytical expressions for the frequency response and amplitude response of a micro-/nano-beam made of the nano-porous biomaterial are proposed for both subharmonic and superharmonic excitations.

2 Analytical approach for mechanical properties of nano-porous biomaterials

In order to simulate a nano-porous biomaterial, it is supposed that it is comprised of truncated cube cells (open cell foam) as depicted in Fig. 1. As a consequence, by placing these cubes beside each other, a unit cell is created. Consequently, the model consists of bigger truncated cube cells and smaller octahedral cells. Figure 2 shows that because of the geometrical symmetry, the links $c_1a_1b_1d_1a_2c_2$ and $c_1a_1b_2d_2a_2c_2$ and $c_1a_1b_3d_3a_2c_2$ and $c_1a_1b_4d_4a_2c_2$ of the unit cell have the same mechanical in-plane deformations. Therefore, it is enough to

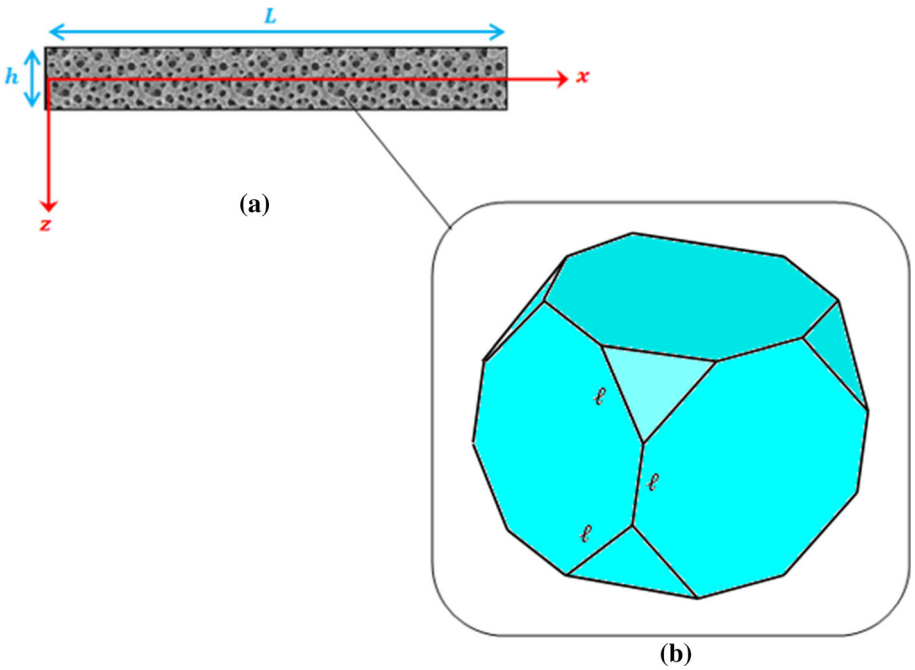

Fig. 1 A micro-/nano-beam made of a nano-porous biomaterial: **a** coordinate system and geometric parameters; **b** a truncated cube lattice framework including struts with length ℓ and circular cross section of radius r

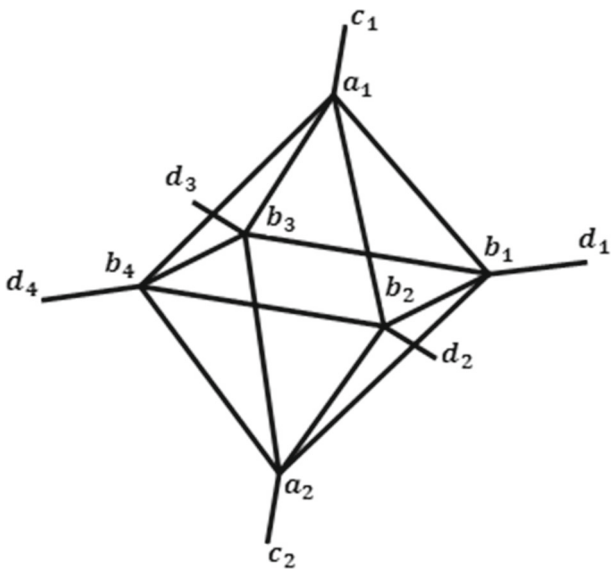

Fig. 2 A schematic representation of a truncated cube unit cell

analyze one of them in order to anticipate the mechanical characteristics of the unit cell. In the current study, the link $c_1a_1b_1d_1a_2c_2$ is selected to be analyzed.

On the basis of the refined hyperbolic shear deformable beam model related to the links of the unit cell, we have

$$\bar{E}\bar{I}\frac{\mathrm{d}^4w}{\mathrm{d}x^4} = \bar{E}\bar{I}\left[\cosh\left(\frac{1}{2}\right) - 12\left(\cosh\left(\frac{1}{2}\right) - 2\sinh\left(\frac{1}{2}\right)\right)\right]\frac{\mathrm{d}^3\psi}{\mathrm{d}x^3} + q\,(x)\,, \tag{1a}$$

$$\bar{E}\bar{I}\left[\cosh\left(\frac{1}{2}\right) - 12\left(\cosh\left(\frac{1}{2}\right) - 2\sinh\left(\frac{1}{2}\right)\right)\right]\frac{\mathrm{d}^3w}{\mathrm{d}x^3}$$

$$= \bar{E}\bar{I}\left[\left(\cosh\left(\frac{1}{2}\right)\right)^2 + 6\left(\sinh(1) - 1\right) - 24\cosh\left(\frac{1}{2}\right)\left(\cosh\left(\frac{1}{2}\right) - 2\sinh\left(\frac{1}{2}\right)\right)\right]\frac{\mathrm{d}^2\psi}{\mathrm{d}x^2}$$
$$-\bar{G}\bar{A}\left[\left(\cosh\left(\frac{1}{2}\right)\right)^2 + \frac{1}{2}\left(\sinh(1) + 1\right) - 4\cosh\left(\frac{1}{2}\right)\sinh\left(\frac{1}{2}\right)\right]\psi, \tag{1b}$$

where $\bar{E}$, $\bar{G}$, $\bar{I}$, $\bar{A}$, w and ψ represent, respectively, the Young's modulus, shear modulus, moment inertia, cross-sectional area, deflection and angle of rotation for the links of unit cell.

Consequently, for a cantilever beam with constructed load P at the free end and length of ℓ, one has

$$\delta_p = w(\ell) = \frac{P\ell^3}{3\bar{E}\bar{I}} + \frac{6}{5}\frac{P\ell}{\bar{G}\bar{A}}\left(1 + \frac{\cosh(p\ell) - \sinh(p\ell) - 1}{p\ell}\right), \tag{2a}$$

$$\theta = \varphi(\ell) = \frac{P\ell^2}{2\bar{E}\bar{I}} + \frac{6}{5}\frac{P}{\bar{G}\bar{A}}\left(1 + \sinh(p\ell) - \cosh(p\ell)\right), \tag{2b}$$

where

$$p = \sqrt{\frac{\frac{\bar{G}\bar{A}}{\bar{E}\bar{I}}\frac{\varsigma_3}{\varsigma_1}}{\frac{\varsigma_2}{\varsigma_1} - \varsigma_1}}, \tag{3}$$

$$\varsigma_1 = \cosh\left(\frac{1}{2}\right) - 12\left[\cosh\left(\frac{1}{2}\right) - 2\sinh\left(\frac{1}{2}\right)\right], \tag{4a}$$

$$\varsigma_2 = \left(\cosh\left(\frac{1}{2}\right)\right)^2 + 6\left[\sinh(1) - 1\right] - 24\cosh\left(\frac{1}{2}\right)\left[\cosh\left(\frac{1}{2}\right) - 2\sinh\left(\frac{1}{2}\right)\right], \tag{4b}$$

$$\varsigma_3 = \left(\cosh\left(\frac{1}{2}\right)\right)^2 + \frac{1}{2}\left[\sinh(1) + 1\right] - 4\cosh\left(\frac{1}{2}\right)\sinh\left(\frac{1}{2}\right). \tag{4c}$$

Based upon the hyperbolic shear deformation beam theory, it is supposed that for the in-plane and transverse displacements, the bending components do not contribute toward shear components and vice versa. Also, there is no need for a shear correction factor which is hard to find its value as it depends on various parameters.

As a result, the equivalent bending moment at the free end of the strut causing the same rotation can be obtained as

$$\frac{P\ell^2}{2\bar{E}\bar{I}} + \frac{6}{5}\frac{P}{\bar{G}\bar{A}}\left(1 + \sinh(p\ell) - \cosh(p\ell)\right) = \frac{M\ell}{\bar{E}\bar{I}} \rightarrow M$$
$$= \frac{P\ell}{2} + \frac{6}{5}\frac{P\bar{E}\bar{I}}{\ell\bar{G}\bar{A}}\left(1 + \sinh(p\ell) - \cosh(p\ell)\right). \tag{5}$$

The associated lateral deflection caused by applying both concentrated load P and bending moment M at the free end can be written as

$$\delta = \delta_P + \delta_M = \frac{P\ell^3}{3\bar{E}\bar{I}} + \frac{6}{5}\frac{P\ell}{\bar{G}\bar{A}}\left(1 + \frac{\cosh(p\ell) - \sinh(p\ell) - 1}{p\ell}\right)$$
$$-\left[\frac{P\ell}{2} + \frac{6}{5}\frac{P\bar{E}\bar{I}}{\ell\bar{G}\bar{A}}\left(1 + \sinh(p\ell) - \cosh(p\ell)\right)\right]\frac{\ell^2}{2\bar{E}\bar{I}}$$
$$= \frac{P\ell^3}{12\bar{E}\bar{I}} + \frac{3}{5}\frac{P\ell}{\bar{G}\bar{A}} + \frac{6}{5}\frac{P\ell}{\bar{G}\bar{A}}\left(\frac{\left(1 + \frac{p\ell}{2}\right)\cosh(p\ell) - \left(1 + \frac{p\ell}{2}\right)\sinh(p\ell) - 1}{p\ell}\right). \tag{6}$$

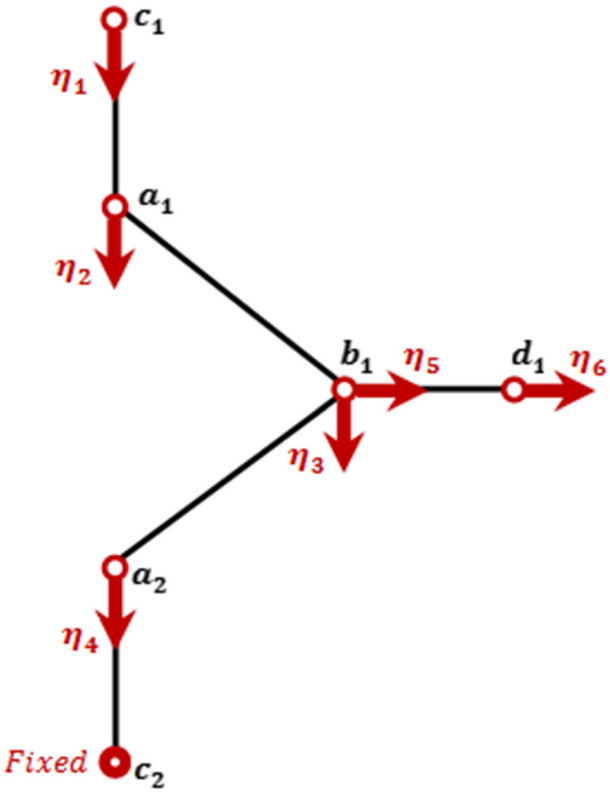

Fig. 3 Degrees of freedom for the link $c_1a_1b_1d_1a_2c_2$ of the unit cell

So, one will have

$$P = \frac{\delta}{\frac{\ell^3}{12\bar{E}\bar{I}} + \frac{3\ell}{5\bar{G}\bar{A}} + \frac{6}{5\bar{G}\bar{A}}\left(\frac{\left(1+\frac{p\ell}{2}\right)\cosh(p\ell)-\left(1+\frac{p\ell}{2}\right)\sinh(p\ell)-1}{p}\right)}. \tag{7}$$

In a general view, the in-plane deformation causes 18 degrees of freedom for the link $c_1a_1b_1d_1a_2c_2$. Nevertheless, the following reasonable assumptions similar to those considered by Hedayati et al. [70] are taken into account in order to decrease the number of degrees of freedom to 6 as illustrated in Fig. 3:

- All the vertices of the links are not enabled to rotate;
- The points a_1, a_2, c_1 are only enabled to displace vertically;
- The vertical displacements of the points b_1 and d_1 are the same, but their horizontal displacements are different;
- The point c_2 is fixed.

Moreover, it is assumed that the porosity is distributed uniformly in the biomaterial, and its shape is similar in all points of the biomaterial.

Consequently, the relationships between the degrees of freedom $x_i (i = 1, 2, \ldots, 6)$ and the associated external force $S_i (i = 1, 2, \ldots, 6)$ can be expressed as

$$\begin{Bmatrix} S_1 \\ S_2 \\ S_3 \\ S_4 \\ S_5 \\ S_6 \end{Bmatrix} = \begin{bmatrix} \mathcal{K}_{11} & \mathcal{K}_{12} & \mathcal{K}_{13} & \mathcal{K}_{14} & \mathcal{K}_{15} & \mathcal{K}_{16} \\ \mathcal{K}_{21} & \mathcal{K}_{22} & \mathcal{K}_{23} & \mathcal{K}_{24} & \mathcal{K}_{25} & \mathcal{K}_{26} \\ \mathcal{K}_{31} & \mathcal{K}_{32} & \mathcal{K}_{33} & \mathcal{K}_{34} & \mathcal{K}_{35} & \mathcal{K}_{36} \\ \mathcal{K}_{41} & \mathcal{K}_{42} & \mathcal{K}_{43} & \mathcal{K}_{44} & \mathcal{K}_{45} & \mathcal{K}_{46} \\ \mathcal{K}_{51} & \mathcal{K}_{52} & \mathcal{K}_{53} & \mathcal{K}_{54} & \mathcal{K}_{55} & \mathcal{K}_{56} \\ \mathcal{K}_{61} & \mathcal{K}_{62} & \mathcal{K}_{63} & \mathcal{K}_{64} & \mathcal{K}_{65} & \mathcal{K}_{66} \end{bmatrix} \begin{Bmatrix} x_1 \\ x_2 \\ x_3 \\ x_4 \\ x_5 \\ x_6 \end{Bmatrix}. \tag{8}$$

Through expression of the displacements corresponding to each degree of freedom separately in such a way that the considered degree of freedom is supposed to be unity and the other ones are assumed to be zero, the elements of the stiffness matrix can be extracted column by column.

For $x_1 = 1$ and $x_2 = x_3 = x_4 = x_5 = x_6 = 0$:

As a result, the point c_1 is displaced downwards by 1 unit. The following associated forces in the struts can be found:

$$S_1 = \frac{2\bar{A}\bar{E}}{\ell}, \quad S_2 = -\frac{2\bar{A}\bar{E}}{\ell}, \quad S_3 = S_4 = S_5 = S_6 = 0. \tag{9}$$

For $x_2 = 1$ and $x_1 = x_3 = x_4 = x_5 = x_6 = 0$:

As a result, the point a_1 (the vertices of links $a_1b_1, a_1b_2, a_1b_3, a_1b_4$) is displaced downwards by 1 unit. The following associated forces in the struts can be found:

$$\begin{aligned}
&S_1 = -\frac{2\bar{A}\bar{E}}{\ell}, \quad S_4 = S_6 = 0,\\
&S_2 = \frac{2\bar{A}\bar{E}}{\ell} + 4 \times \left(\frac{1}{\frac{\ell^3}{6\bar{E}\bar{I}} + \frac{6\ell}{5\bar{G}\bar{A}} + \frac{12}{5\bar{G}\bar{A}} \left(\frac{\left(1+\frac{p\ell}{2}\right)\cosh(p\ell) - \left(1+\frac{p\ell}{2}\right)\sinh(p\ell) - 1}{p} \right)} + \frac{\bar{A}\bar{E}}{2\ell} \right),\\
&S_3 = -4 \times \left(\frac{1}{\frac{\ell^3}{6\bar{E}\bar{I}} + \frac{6\ell}{5\bar{G}\bar{A}} + \frac{12}{5\bar{G}\bar{A}} \left(\frac{\left(1+\frac{p\ell}{2}\right)\cosh(p\ell) - \left(1+\frac{p\ell}{2}\right)\sinh(p\ell) - 1}{p} \right)} + \frac{\bar{A}\bar{E}}{2\ell} \right),\\
&S_5 = 4 \times \left(\frac{1}{\frac{\ell^3}{6\bar{E}\bar{I}} + \frac{6\ell}{5\bar{G}\bar{A}} + \frac{12}{5\bar{G}\bar{A}} \left(\frac{\left(1+\frac{p\ell}{2}\right)\cosh(p\ell) - \left(1+\frac{p\ell}{2}\right)\sinh(p\ell) - 1}{p} \right)} - \frac{\bar{A}\bar{E}}{2\ell} \right).
\end{aligned} \tag{10}$$

For $x_3 = 1$ and $x_1 = x_2 = x_4 = x_5 = x_6 = 0$:

As a result, the point b_1 (similarly, the points b_2, b_3, b_4) is displaced downwards by 1 unit. The associated forces in the struts become

$$\begin{aligned}
&S_1 = S_5 = S_6 = 0,\\
&S_2 = S_4 = -4 \times \left(\frac{1}{\frac{\ell^3}{6\bar{E}\bar{I}} + \frac{6\ell}{5\bar{G}\bar{A}} + \frac{12}{5\bar{G}\bar{A}} \left(\frac{\left(1+\frac{p\ell}{2}\right)\cosh(p\ell) - \left(1+\frac{p\ell}{2}\right)\sinh(p\ell) - 1}{p} \right)} - \frac{\bar{A}\bar{E}}{2\ell} \right),\\
&S_3 = 4 \times \left(\frac{1}{\frac{\ell^3}{12\bar{E}\bar{I}} + \frac{3\ell}{5\bar{G}\bar{A}} + \frac{6}{5\bar{G}\bar{A}} \left(\frac{\left(1+\frac{p\ell}{2}\right)\cosh(p\ell) - \left(1+\frac{p\ell}{2}\right)\sinh(p\ell) - 1}{p} \right)} + \frac{\bar{A}\bar{E}}{\ell} \right).
\end{aligned} \tag{11}$$

For $x_4 = 1$ and $x_1 = x_2 = x_3 = x_5 = x_6 = 0$:

As a result, the point a_2 (the vertices of links $a_2b_1, a_2b_2, a_2b_3, a_2b_4$) is displaced downwards by 1 unit. The associated forces in the struts are as follows:

$$S_1 = S_2 = S_6 = 0,$$

$$S_3 = -4 \times \left(\frac{1}{\frac{\ell^3}{6\bar{E}\bar{I}} + \frac{6\ell}{5\bar{G}\bar{A}} + \frac{12}{5\bar{G}\bar{A}} \left(\frac{\left(1+\frac{p\ell}{2}\right)\cosh(p\ell) - \left(1+\frac{p\ell}{2}\right)\sinh(p\ell) - 1}{p} \right)} + \frac{\bar{A}\bar{E}}{2\ell} \right),$$

$$S_4 = \frac{2\bar{A}\bar{E}}{\ell} + 4 \times \left(\frac{1}{\frac{\ell^3}{6\bar{E}\bar{I}} + \frac{6\ell}{5\bar{G}\bar{A}} + \frac{12}{5\bar{G}\bar{A}} \left(\frac{\left(1+\frac{p\ell}{2}\right)\cosh(p\ell) - \left(1+\frac{p\ell}{2}\right)\sinh(p\ell) - 1}{p} \right)} + \frac{\bar{A}\bar{E}}{2\ell} \right),$$

$$S_5 = -4 \times \left(\frac{1}{\frac{\ell^3}{6\bar{E}\bar{I}} + \frac{6\ell}{5\bar{G}\bar{A}} + \frac{12}{5\bar{G}\bar{A}} \left(\frac{\left(1+\frac{p\ell}{2}\right)\cosh(p\ell) - \left(1+\frac{p\ell}{2}\right)\sinh(p\ell) - 1}{p} \right)} - \frac{\bar{A}\bar{E}}{2\ell} \right). \tag{12}$$

For $x_5 = 1$ and $x_1 = x_2 = x_3 = x_4 = x_6 = 0$:
As a result, the point b_1 (similarly, the points b_2, b_3, b_4) is displaced horizontally by 1 unit. The associated forces in the struts can be given as

$$S_1 = S_3 = 0,$$

$$S_2 = 4 \times \left(\frac{1}{\frac{\ell^3}{6\bar{E}\bar{I}} + \frac{6\ell}{5\bar{G}\bar{A}} + \frac{12}{5\bar{G}\bar{A}} \left(\frac{\left(1+\frac{p\ell}{2}\right)\cosh(p\ell) - \left(1+\frac{p\ell}{2}\right)\sinh(p\ell) - 1}{p} \right)} - \frac{\bar{A}\bar{E}}{2\ell} \right),$$

$$S_4 = -4 \times \left(\frac{1}{\frac{\ell^3}{6\bar{E}\bar{I}} + \frac{6\ell}{5\bar{G}\bar{A}} + \frac{12}{5\bar{G}\bar{A}} \left(\frac{\left(1+\frac{p\ell}{2}\right)\cosh(p\ell) - \left(1+\frac{p\ell}{2}\right)\sinh(p\ell) - 1}{p} \right)} - \frac{\bar{A}\bar{E}}{2\ell} \right),$$

$$S_5 = 4 \times \left(\frac{1}{\frac{\ell^3}{12\bar{E}\bar{I}} + \frac{3\ell}{5\bar{G}\bar{A}} + \frac{6}{5\bar{G}\bar{A}} \left(\frac{\left(1+\frac{p\ell}{2}\right)\cosh(p\ell) - \left(1+\frac{p\ell}{2}\right)\sinh(p\ell) - 1}{p} \right)} + \frac{5\bar{A}\bar{E}}{\ell} \right),$$

$$S_6 = -4 \times \left(\frac{2\bar{A}\bar{E}}{\ell} \right). \tag{13}$$

For $x_6 = 1$ and $x_1 = x_2 = x_3 = x_4 = x_5 = 0$:
As a result, the point d_1 (similarly, the points d_2, d_3, d_4) is displaced horizontally by 1 unit. The associated forces in the struts can be expressed as:

$$S_1 = S_2 = S_3 = S_4 = 0,$$
$$S_5 = -4 \left(\frac{2\bar{A}\bar{E}}{\ell} \right),$$
$$S_6 = 4 \left(\frac{2\bar{A}\bar{E}}{\ell} \right). \tag{14}$$

Equation (8) leads to the elements of the stiffness matrix which are given in Appendix A.

As was mentioned by Hedayati et al. [70], it is assumed that the external force, P, acts vertically on point c_1 of the refined truncated cube lattice structure, which causes an additional horizontal force equal to $\frac{8\bar{A}\bar{E}(x_6-x_5)}{\ell}$ at point d_1. This yields

$$\begin{Bmatrix} P \\ 0 \\ 0 \\ 0 \\ 0 \\ 0 \end{Bmatrix} = \begin{bmatrix} \mathcal{K}_{11} & \mathcal{K}_{12} & 0 & 0 & 0 & 0 \\ \mathcal{K}_{21} & \mathcal{K}_{22} & \mathcal{K}_{23} & 0 & \mathcal{K}_{25} & 0 \\ 0 & \mathcal{K}_{32} & \mathcal{K}_{33} & \mathcal{K}_{34} & 0 & 0 \\ 0 & 0 & \mathcal{K}_{43} & \mathcal{K}_{44} & \mathcal{K}_{45} & 0 \\ 0 & \mathcal{K}_{52} & 0 & \mathcal{K}_{54} & \mathcal{K}_{55} & \mathcal{K}_{56} \\ 0 & 0 & 0 & 0 & 2\mathcal{K}_{65} & 2\mathcal{K}_{66} \end{bmatrix} \begin{Bmatrix} x_1 \\ x_2 \\ x_3 \\ x_4 \\ x_5 \\ x_6 \end{Bmatrix}. \tag{15}$$

It should be noted that a simpler version of the unit cell used here in the lattice structure of porous materials has been studied previously by Sun et al. [71] and Yang [72], where the horizontal struts (struts b_1b_2, b_2b_3, b_3b_4, b_4b_1 shown in Fig. 2) as important factors for the structural strength are excluded. The presence of this horizontal struts has the advantage of an approximately isotropic homogenization for the lattice structure. Consequently, as it is depicted in Fig. 3, for instance, the links of the present unit cell in the lattice structure are geometrically similar. (The square $b_1b_2b_3b_4$ is the symmetric plane of the unit cell.) Consequently, the elastic modulus of the truncated cube unit cell can be calculated as

$$E = \frac{F_{\mathrm{u}}L_{\mathrm{u}}}{A_{\mathrm{u}}\delta_{\mathrm{u}}} = \frac{P}{\left(1+\sqrt{2}\right)\ell x_1}, \tag{16}$$

where F_{u}, L_{u}, A_{u} and δ_{u} denote, respectively, the applied load, length, cross-sectional area and shortening of the unit cell.

After that, inversion of Eq. (16) results in x_1 as a function of P. Therefore, after some mathematical calculations, it can be written as

$$\begin{aligned} E = \Big(&\mathcal{K}_{11}+\mathcal{K}_{22}\mathcal{K}_{33}\mathcal{K}_{66}\mathcal{K}_{45}\mathcal{K}_{54}-\mathcal{K}_{11}+\mathcal{K}_{22}\mathcal{K}_{33}\mathcal{K}_{44}\mathcal{K}_{55}\mathcal{K}_{66}+\mathcal{K}_{11}+\mathcal{K}_{22}\mathcal{K}_{55}\mathcal{K}_{66}\mathcal{K}_{34}\mathcal{K}_{43} \\ &+\mathcal{K}_{11}\mathcal{K}_{33}\mathcal{K}_{44}\mathcal{K}_{66}\mathcal{K}_{25}\mathcal{K}_{52}-\mathcal{K}_{11}\mathcal{K}_{66}\mathcal{K}_{25}\mathcal{K}_{52}\mathcal{K}_{34}\mathcal{K}_{43}+2\mathcal{K}_{11}\mathcal{K}_{66}\mathcal{K}_{34}\mathcal{K}_{45}\mathcal{K}_{23}\mathcal{K}_{25} \\ &+\mathcal{K}_{11}\mathcal{K}_{44}\mathcal{K}_{55}\mathcal{K}_{66}\mathcal{K}_{23}\mathcal{K}_{32}-\mathcal{K}_{11}\mathcal{K}_{66}\mathcal{K}_{45}\mathcal{K}_{54}\mathcal{K}_{23}\mathcal{K}_{32}+\mathcal{K}_{33}\mathcal{K}_{44}\mathcal{K}_{55}\mathcal{K}_{66}\mathcal{K}_{12}\mathcal{K}_{21} \\ &-\mathcal{K}_{33}\mathcal{K}_{66}\mathcal{K}_{45}\mathcal{K}_{54}\mathcal{K}_{12}\mathcal{K}_{21}-\mathcal{K}_{55}\mathcal{K}_{66}\mathcal{K}_{12}\mathcal{K}_{21}\mathcal{K}_{34}\mathcal{K}_{43}+\mathcal{K}_{11}\mathcal{K}_{22}\mathcal{K}_{33}\mathcal{K}_{44}\mathcal{K}_{56}\mathcal{K}_{65} \\ &-\mathcal{K}_{33}\mathcal{K}_{44}\mathcal{K}_{12}\mathcal{K}_{21}\mathcal{K}_{56}\mathcal{K}_{65}-\mathcal{K}_{11}\mathcal{K}_{44}\mathcal{K}_{23}\mathcal{K}_{32}\mathcal{K}_{56}\mathcal{K}_{65}-\mathcal{K}_{11}\mathcal{K}_{22}\mathcal{K}_{34}\mathcal{K}_{43}\mathcal{K}_{56}\mathcal{K}_{65} \\ &+\mathcal{K}_{12}\mathcal{K}_{21}\mathcal{K}_{34}\mathcal{K}_{43}\mathcal{K}_{56}\mathcal{K}_{65}\Big)\Big/\Big[(\mathcal{K}_{66}\mathcal{K}_{22}\mathcal{K}_{33}\mathcal{K}_{45}\mathcal{K}_{54}-\mathcal{K}_{66}\mathcal{K}_{22}\mathcal{K}_{33}\mathcal{K}_{55}\mathcal{K}_{44} \\ &+\mathcal{K}_{22}\mathcal{K}_{55}\mathcal{K}_{66}\mathcal{K}_{34}\mathcal{K}_{43}+\mathcal{K}_{33}\mathcal{K}_{44}\mathcal{K}_{66}\mathcal{K}_{25}\mathcal{K}_{52}-\mathcal{K}_{66}\mathcal{K}_{25}\mathcal{K}_{52}\mathcal{K}_{34}\mathcal{K}_{43} \\ &+2\mathcal{K}_{66}\mathcal{K}_{45}\mathcal{K}_{34}\mathcal{K}_{23}\mathcal{K}_{25}+\mathcal{K}_{44}\mathcal{K}_{55}\mathcal{K}_{66}\mathcal{K}_{23}\mathcal{K}_{32}-\mathcal{K}_{66}\mathcal{K}_{45}\mathcal{K}_{54}\mathcal{K}_{23}\mathcal{K}_{32} \\ &+\mathcal{K}_{22}\mathcal{K}_{33}\mathcal{K}_{44}\mathcal{K}_{56}\mathcal{K}_{65}-\mathcal{K}_{44}\mathcal{K}_{23}\mathcal{K}_{32}\mathcal{K}_{56}\mathcal{K}_{65}-\mathcal{K}_{22}\mathcal{K}_{34}\mathcal{K}_{43}\mathcal{K}_{56}\mathcal{K}_{65})(1+\sqrt{2})\ell\Big]. \end{aligned} \tag{17}$$

In addition, to capture the Poisson's ratio of the nano-porous biomaterial, it can be defined as the ratio of horizontal to vertical displacements of the unit cell as follows:

$$\nu = \frac{2x_6}{x_1}. \tag{18}$$

Therefore, it can be rewritten as

$$\begin{aligned} \nu = &2\mathcal{K}_{12}\mathcal{K}_{56}(\mathcal{K}_{33}\mathcal{K}_{44}\mathcal{K}_{25}-\mathcal{K}_{25}\mathcal{K}_{34}\mathcal{K}_{43}+\mathcal{K}_{23}\mathcal{K}_{34}\mathcal{K}_{45})/(\mathcal{K}_{22}\mathcal{K}_{33}\mathcal{K}_{66}\mathcal{K}_{45}\mathcal{K}_{54} \\ &-\mathcal{K}_{22}\mathcal{K}_{33}\mathcal{K}_{44}\mathcal{K}_{55}\mathcal{K}_{66}+\mathcal{K}_{22}\mathcal{K}_{55}\mathcal{K}_{66}\mathcal{K}_{34}\mathcal{K}_{43}+\mathcal{K}_{33}\mathcal{K}_{44}\mathcal{K}_{66}\mathcal{K}_{25}\mathcal{K}_{52} \\ &-\mathcal{K}_{66}\mathcal{K}_{25}\mathcal{K}_{52}\mathcal{K}_{34}\mathcal{K}_{43}+2\mathcal{K}_{66}\mathcal{K}_{23}\mathcal{K}_{25}\mathcal{K}_{34}\mathcal{K}_{45}+\mathcal{K}_{44}\mathcal{K}_{55}\mathcal{K}_{66}\mathcal{K}_{23}\mathcal{K}_{32} \\ &-\mathcal{K}_{66}\mathcal{K}_{23}\mathcal{K}_{32}\mathcal{K}_{45}\mathcal{K}_{54}+\mathcal{K}_{22}\mathcal{K}_{33}\mathcal{K}_{44}\mathcal{K}_{56}\mathcal{K}_{65}-\mathcal{K}_{44}\mathcal{K}_{23}\mathcal{K}_{32}\mathcal{K}_{56}\mathcal{K}_{65} \\ &+\mathcal{K}_{22}\mathcal{K}_{34}\mathcal{K}_{43}\mathcal{K}_{56}\mathcal{K}_{65}). \end{aligned} \tag{19}$$

Additionally, the material overlay in the vertices can be removed with the aid of the method of mass multiple counting proposed by Hedayati et al. [73], so the mass density of the nano-porous biomaterial including truncated cube cells can be evaluated as a function of the pore size (ℓ/r) as follows:

$$\rho = V^* \bar{\rho} = \frac{24\left(\frac{\pi}{2}\frac{\ell}{r} - 2.5758\right) + 12\left(\frac{\pi}{4}\frac{\ell}{r} - 1.2879\right)}{\left(1+\sqrt{2}\right)^3 \left(\frac{\ell}{r}\right)^3}\bar{\rho}, \tag{20}$$

where $\bar{\rho}$ is the mass density of the material without porosity and V^* is the ratio of the occupied volume of the complete cube to the occupied volume of the truncated cube.

At this point should be noted that in the current study, it is assumed that ℓ/r represents the influence of the porosity on the ratio of the volume occupied by the material to the total volume of the unit cell, so it is named as pore size.

3 Size-dependent modeling of a micro-/nano-beam made of nano-porous biomaterial

The components of the displacement vector along different coordinate directions for a beam-type structure as shown in Fig. 1 take the following form:

$$u_x(x,t) = u(x,t) - z\frac{\partial w(x,t)}{\partial x}, \tag{21a}$$

$$u_z(x,t) = w(x,t), \tag{21b}$$

in which u and w are the scalar displacement parameters of the micro-/nano-beam along the x- and z-axes, respectively.

Accordingly, the nonzero nonlinear strain component can be given as

$$\varepsilon_{xx} = \frac{\partial u}{\partial x} - z\frac{\partial^2 w}{\partial x^2} + \frac{1}{2}\left(\frac{\partial w}{\partial x}\right)^2. \tag{22}$$

In order to incorporate simultaneously both hardening-stiffness and softening-stiffness influences of size dependency at nanoscale, Lim et al. [51] proposed a new size-dependent continuum theory of elasticity, namely the nonlocal strain gradient elasticity theory. In accordance with this theory, the strain energy of a nano-structure can be evaluated as

$$\Pi_s = \frac{1}{2}\int_V \left\{\sigma_{ij}\varepsilon_{ij} + \sigma^*_{ij}\varepsilon_{ij,k}\right\} \mathrm{d}V, \tag{23}$$

where σ_{ij} and σ^*_{ij} are, respectively, the nonlocal and higher-order nonlocal stress tensors which can be introduced as

$$\sigma_{ij} = \int_V \left\{\varrho_1\left(\left|\mathcal{X}' - \mathcal{X}\right|, \mu\right) C_{ijkl}\varepsilon_{ij}\right\} \mathrm{d}V, \tag{24a}$$

$$\sigma^*_{ij} = l^2\int_V \left\{\varrho_2\left(\left|\mathcal{X}' - \mathcal{X}\right|, \mu\right) C_{ijkl}\varepsilon_{ij,k}\right\} \mathrm{d}V, \tag{24b}$$

in which l denotes the strain gradient parameter to consider the deformation at microscale, ϱ_1 and ϱ_2 are the attenuation nonlocal kernel functions associated with the classical and strain gradient stress tensors, respectively. Also, C is the elasticity matrix, $\mathcal{X}$ and $\mathcal{X}'$ in order represent a point and any point else in the body, μ stands for the nonlocal parameter.

Following the method of Eringen, the nonclassical stress–strain relationships become

$$\left(1 - \mu^2\nabla^2\right)\sigma_{ij} = C_{ijkl}\varepsilon_{kl}, \tag{25a}$$

$$\left(1 - \mu^2\nabla^2\right)\sigma^*_{ij} = l^2 C_{ijkl}\varepsilon_{kl,m}, \tag{25b}$$

in which μ is the nonlocal parameter.

On the other hand, based upon the nonlocal strain gradient theory of elasticity, the constitutive relationship corresponding to the total nonlocal strain gradient stress tensor can be expressed as

$$\mathcal{T}_{ij} = \sigma_{ij} - \nabla\sigma^*_{ij}. \tag{26}$$

As a result, the general nonlocal strain gradient constitutive equation can be written as

$$\left(1-\mu^2\nabla^2\right)\mathcal{T}_{ij}=C_{ijkl}\left(1-l^2\nabla^2\right)\varepsilon_{kl}. \tag{27}$$

For a beam-type structure, one has

$$\left(1-\mu^2\frac{\partial^2}{\partial x^2}\right)\mathcal{T}_{xx}=\left(\frac{E}{1-\nu^2}\right)\left(\frac{\partial u}{\partial x}-z\frac{\partial^2 w}{\partial x^2}+\frac{1}{2}\left(\frac{\partial w}{\partial x}\right)^2\right)$$
$$-\left(\frac{E}{1-\nu^2}\right)l^2\frac{\partial^2}{\partial x^2}\left(\frac{\partial u}{\partial x}-z\frac{\partial^2 w}{\partial x^2}+\frac{1}{2}\left(\frac{\partial w}{\partial x}\right)^2\right). \tag{28}$$

Thus, the strain energy associated with a micro-/nano-beam on the basis of the nonlocal strain gradient elasticity theory can be obtained as

$$\Pi_{\mathrm{s}}=\frac{1}{2}\int_0^L\left\{N_{xx}\left(\frac{\partial u}{\partial x}+\frac{1}{2}\left(\frac{\partial w}{\partial x}\right)^2\right)-M_{xx}\frac{\partial^2 w}{\partial x^2}\right\}\mathrm{d}x, \tag{29}$$

where the stress resultants are in the following forms:

$$N_{xx}-\mu^2\frac{\partial^2 N_{xx}}{\partial x^2}=A_{11}\left(1-l^2\frac{\partial^2}{\partial x^2}\right)\left(\frac{\partial u}{\partial x}+\frac{1}{2}\left(\frac{\partial w}{\partial x}\right)^2\right), \tag{30a}$$

$$M_{xx}-\mu^2\frac{\partial^2 M_{xx}}{\partial x^2}=-D_{11}\left(1-l^2\frac{\partial^2}{\partial x^2}\right)\frac{\partial^2 w}{\partial x^2}, \tag{30b}$$

where

$$\{N_{xx},M_{xx}\}=b\int_{-\frac{h}{2}}^{\frac{h}{2}}\mathcal{T}_{xx}\{1,z\}\,dz,$$
$$\{A_{11},D_{11}\}=\frac{Eb}{1-\nu^2}\int_{-\frac{h}{2}}^{\frac{h}{2}}\left\{1,z^2\right\}dz=\left\{\frac{Ebh}{1-\nu^2},\frac{Ebh^3}{12\left(1-\nu^2\right)}\right\}. \tag{31}$$

Moreover, the kinematic energy of the micro-/nano-beam can be defined as

$$\Pi_T=\frac{1}{2}\int_V\rho\left\{\left(\frac{\partial u_x}{\partial t}\right)^2+\left(\frac{\partial u_z}{\partial t}\right)^2\right\}\mathrm{d}V$$
$$=\frac{1}{2}\int_x\left\{\rho bh\left(\frac{\partial u}{\partial t}\right)^2+\rho bh\left(\frac{\partial w}{\partial t}\right)^2+\frac{\rho bh^3}{12}\left(\frac{\partial^2 w}{\partial x\partial t}\right)^2\right\}\mathrm{d}x. \tag{32}$$

Additionally, the work done by the external distributed load f can be given as

$$\Pi_P=\int_x f\,(x,t)\,w\mathrm{d}x. \tag{33}$$

Using Hamilton's principle, one obtains the following differential equations

$$\frac{\partial N_{xx}}{\partial x}=I_1\frac{\partial^2 u}{\partial t^2}, \tag{34a}$$

$$\frac{\partial}{\partial x}\left[N_{xx}\frac{\partial w}{\partial x}\right]+\frac{\partial^2 M_{xx}}{\partial x^2}=f+I_1\frac{\partial^2 w}{\partial t^2}-I_3\frac{\partial^4 w}{\partial x^2\partial t^2}, \tag{34b}$$

in which

$$\{I_1,I_3\}=b\int_{-\frac{h}{2}}^{\frac{h}{2}}\rho\left\{1,z^2\right\}dz=\left\{\rho bh,\frac{\rho bh^3}{12}\right\}. \tag{35}$$

In the fast dynamic problem, it can be assumed that $\frac{\partial^2 u}{\partial t^2} = 0$. Therefore, based on Eq. (34a), one will have $N_{xx} = c$, where c is a constant. In addition, for immovable end supports, this yields

$$N_{xx} = \frac{A_{11}}{2L}\int_0^L \left(\frac{\partial w}{\partial x}\right)^2 \mathrm{d}x. \tag{36}$$

Consequently, Eq. (34b) can be expressed in terms of the displacement field as follows:

$$\begin{aligned} &-D_{11}\left(1-l^2\frac{\partial^2}{\partial x^2}\right)\frac{\partial^4 w}{\partial x^4} + \left[\frac{A_{11}}{2L}\int_0^L \left(\frac{\partial w}{\partial x}\right)^2 \mathrm{d}x\right]\left(1-\mu^2\frac{\partial^2}{\partial x^2}\right)\frac{\partial^2 w}{\partial x^2} \\ &\quad = \left(1-\mu^2\frac{\partial^2}{\partial x^2}\right)\left(f + I_1\frac{\partial^2 w}{\partial t^2} - I_3\frac{\partial^4 w}{\partial x^2 \partial t^2}\right). \end{aligned} \tag{37}$$

It should be mentioned here that the nonlocal stress and strain gradient size dependencies are taken into account via the unconventional continuum theories applied to the stress–strain constitutive equations of the micro-/nano-structure. As a result, the material properties are the same based on both classical (local) and nonlocal strain gradient elasticity theories, and they are independent of the size effects. Therefore, in the analytical solution for capturing the material properties of the porous material properties, the classical (local) elasticity is put to use. But for the vibrational resonance analysis of the micro-/nano-beam made of this porous material, the size effects are considered based upon the nonlocal strain gradient theory of elasticity.

4 Multiple-timescale solving process

In order to perform the solution process in a more general form, the following dimensionless parameters are introduced:

$$\begin{aligned} &W = \frac{w}{h}, \quad X = \frac{x}{L}, \quad \vartheta = \frac{h}{L}, \quad T = \frac{t}{L}\sqrt{\frac{E_0}{\rho_0}}, \quad \left\{\hat{I}_1, \hat{I}_3\right\} = \left\{\frac{I_1}{\rho_0 bh}, \frac{I_3}{\rho_0 bh^3}\right\}, \\ &F = \frac{fL^2}{E_0 bh^2}, \quad a_{11} = \frac{A_{11}}{E_0 bh}, \quad d_{11} = \frac{D_{11}}{E_0 bh^3}, \quad \mathcal{G}_1 = \frac{l}{L}, \quad \mathcal{G}_2 = \frac{\mu}{L}, \end{aligned} \tag{38}$$

where E_0 and ρ_0 are the Young's modulus and mass density of the nano-porous biomaterial with a pore size of $\ell/r = 10$.

Therefore, the dimensionless form of the size-dependent nonlinear governing differential equation of motion takes the following form:

$$\begin{aligned} &-d_{11}\vartheta^2\left(1-\mathcal{G}_1^2\frac{\partial^2}{\partial X^2}\right)\frac{\partial^4 W}{\partial X^4} + \left[\frac{a_{11}\vartheta^2}{2}\int_0^1 \left(\frac{\partial W}{\partial X}\right)^2 \mathrm{d}x\right]\left(1-\mathcal{G}_2^2\frac{\partial^2}{\partial X^2}\right)\frac{\partial^2 W}{\partial X^2} \\ &\quad = \left(1-\mathcal{G}_2^2\frac{\partial^2}{\partial X^2}\right)\left(F + \hat{I}_1\frac{\partial^2 W}{\partial T^2} - \hat{I}_3\vartheta^2\frac{\partial^4 W}{\partial X^2 \partial T^2}\right). \end{aligned} \tag{39}$$

With the aid of the Galerkin technique, the governing differential equation can be written in discretized form. To this end, it is assumed that $W(X, T)$ can be expressed separately as

$$W(X, T) = \varphi(X)\, q(T). \tag{40}$$

By inserting Eq. (40) into Eq. (39), one obtains

$$\begin{aligned} &-d_{11}\vartheta^2 q\left(\frac{\mathrm{d}^4\varphi}{\mathrm{d}x^4} - \mathcal{G}_1^2\frac{\mathrm{d}^6\varphi}{\mathrm{d}x^6}\right) + \frac{a_{11}\vartheta^2 q^3}{2}\left[\int_0^1 \left(\frac{d\varphi}{\mathrm{d}x}\right)^2 \mathrm{d}x\right]\left(\frac{\mathrm{d}^2\varphi}{\mathrm{d}x^2} - \mathcal{G}_2^2\frac{\mathrm{d}^4\varphi}{\mathrm{d}X^4}\right) \\ &\quad = F - \mathcal{G}_2^2\frac{\partial^2 F}{\partial X^2} + \hat{I}_1\left(\varphi\frac{\mathrm{d}^2 q}{\mathrm{d}T^2} - \mathcal{G}_2^2\frac{\mathrm{d}^2\varphi}{\mathrm{d}X^2}\frac{\mathrm{d}^2 q}{\mathrm{d}T^2}\right) - \hat{I}_3\vartheta^2\left(\frac{\mathrm{d}^2\varphi}{\mathrm{d}X^2}\frac{dq^2}{\mathrm{d}T^2} - \mathcal{G}_2^2\frac{\mathrm{d}^4\varphi}{\mathrm{d}X^4}\frac{\mathrm{d}^2 q}{\mathrm{d}T^2}\right). \end{aligned} \tag{41}$$

By employing the Galerkin technique, the Duffing type equation of motion can be extracted in the form

$$\ddot{q} + 2\beta\dot{q} + \omega^2 q + \alpha q^3 = \tilde{F}, \tag{42}$$

in which

$$\begin{aligned}
\omega^2 &= -\frac{\int_0^1 \left\{-d_{11}\vartheta^2\varphi\left(\frac{\mathrm{d}^4\varphi}{\mathrm{d}X^4} - \mathcal{G}_1^2\frac{\mathrm{d}^6\varphi}{\mathrm{d}X^6}\right)\right\}\mathrm{d}X}{\int_0^1 \left\{\hat{I}_1\varphi\left(\varphi - \mathcal{G}_2^2\frac{\mathrm{d}^2\varphi}{\mathrm{d}X^2}\right) - \hat{I}_3\vartheta^2\varphi\left(\frac{\mathrm{d}^2\varphi}{\mathrm{d}X^2} - \mathcal{G}_2^2\frac{\mathrm{d}^4\varphi}{\mathrm{d}X^4}\right)\right\}\mathrm{d}X}, \\
\alpha &= -\frac{\int_0^1 \left\{\frac{a_{11}\vartheta^2\varphi}{2}\left[\int_0^1\left(\frac{d\varphi}{\mathrm{d}X}\right)^2\mathrm{d}X\right]\left(\frac{\mathrm{d}^2\varphi}{\mathrm{d}X^2} - \mathcal{G}_2^2\frac{\mathrm{d}^4\varphi}{\mathrm{d}X^4}\right)\right\}\mathrm{d}X}{\int_0^1 \left\{\hat{I}_1\varphi\left(\varphi - \mathcal{G}_2^2\frac{\mathrm{d}^2\varphi}{\mathrm{d}X^2}\right) - \hat{I}_3\vartheta^2\varphi\left(\frac{\mathrm{d}^2\varphi}{\mathrm{d}X^2} - \mathcal{G}_2^2\frac{\mathrm{d}^4\varphi}{\mathrm{d}X^4}\right)\right\}\mathrm{d}X}, \\
\tilde{F} &= -\frac{F - \mathcal{G}_2^2\frac{\partial^2 F}{\partial X^2}}{\int_0^1 \left\{\hat{I}_1\varphi\left(\varphi - \mathcal{G}_2^2\frac{\mathrm{d}^2\varphi}{\mathrm{d}X^2}\right) - \hat{I}_3\vartheta^2\varphi\left(\frac{\mathrm{d}^2\varphi}{\mathrm{d}X^2} - \mathcal{G}_2^2\frac{\mathrm{d}^4\varphi}{\mathrm{d}X^4}\right)\right\}\mathrm{d}X}.
\end{aligned} \tag{43}$$

Also, it is assumed that the external distributed load is a dissipative one, so the damping parameter takes the form

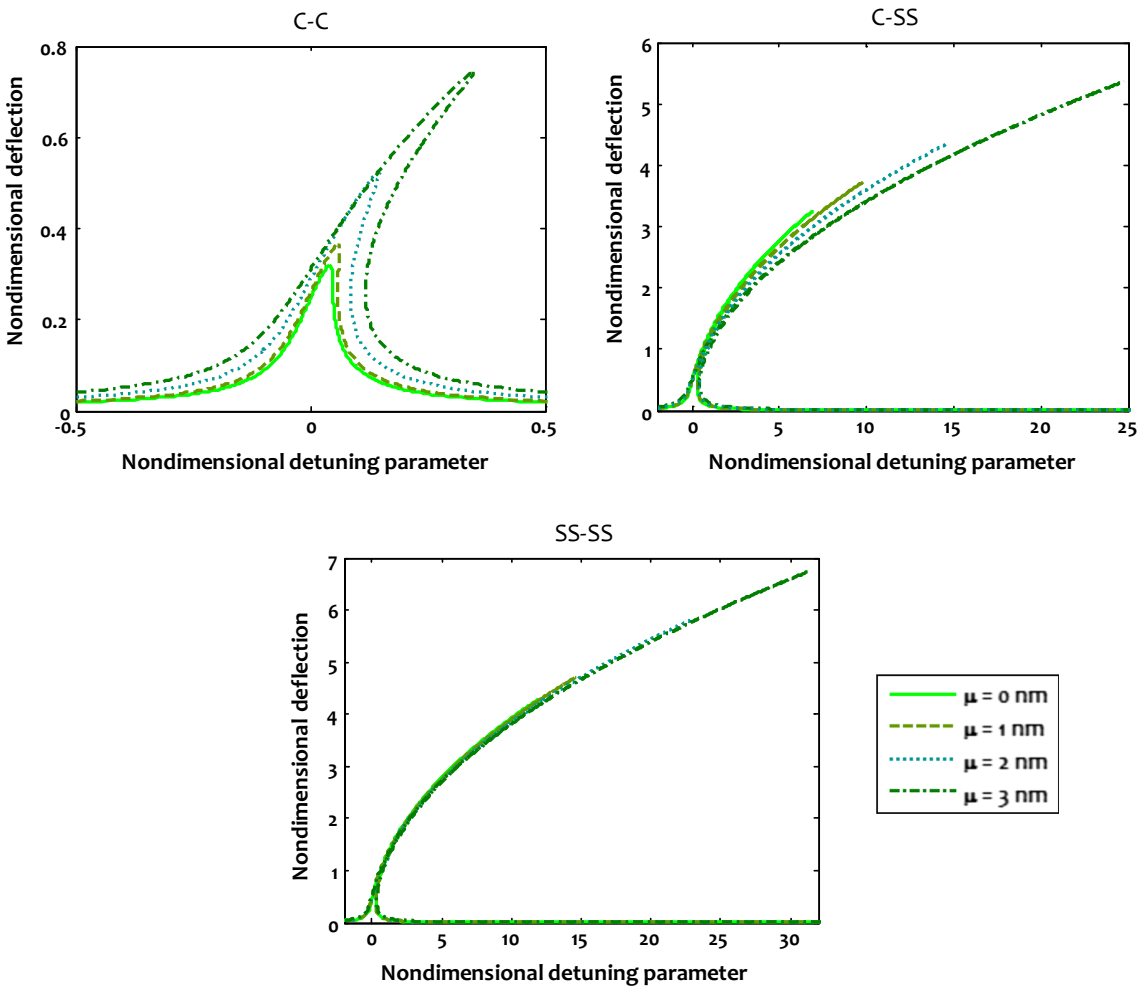

Fig. 4 Size-dependent frequency response of the micro-/nano-beam under superharmonic excitation corresponding to different nonlocal parameters and boundary conditions ($l = 0$ nm)

$$\beta = \frac{\eta\omega^2}{\omega_{\mathrm{L}}}, \tag{44}$$

where ω_{L} represents the linear frequency of the system and η is a constant.

The analytical expression for $\varphi(X)$ corresponding to each type of boundary conditions can be introduced as [74]

- For simply supported–simply supported boundary conditions:

$$\varphi(X) = \sin(\pi X) \tag{45}$$

- For clamped–clamped boundary conditions:

$$\varphi(X) = \cos(4.73X) - \cosh(4.73X) + \left(\frac{\cos(4.73) - \cosh(4.73)}{\sin(4.73) - \sinh(4.73)}\right)(\sinh(4.73X) - \sin(4.73X)) \tag{46}$$

- For simply supported–clamped boundary conditions:

$$\varphi(X) = \cos(3.927X) - \cosh(3.927X) + \left(\frac{\cos(3.927) - \cosh(3.927)}{\sin(3.927) - \sinh(3.927)}\right)(\sinh(3.927X) - \sin(3.927X)) \tag{47}$$

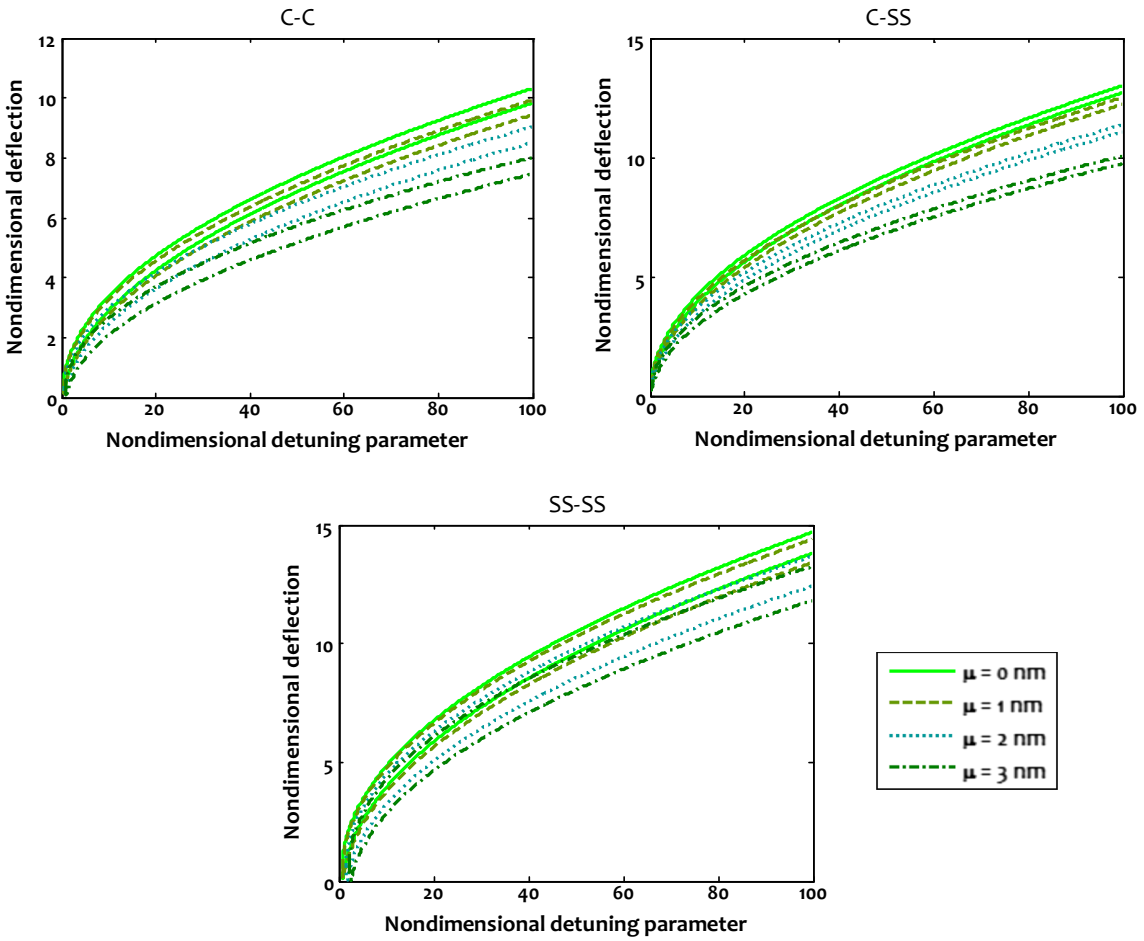

Fig. 5 Size-dependent frequency response of the micro-/nano-beam under subharmonic excitation corresponding to different nonlocal parameters and boundary conditions ($l = 0$ nm)

The damping and nonlinear terms are supposed to be small and they are in the order of a small parameter, ϵ. Consequently, Eq. (42) takes the following form:

$$\ddot{q} + 2\beta\epsilon\dot{q} + \omega^2 q + \alpha\epsilon q^3 = \tilde{F}. \tag{48}$$

For the hard excitation, the order of the external distributed load is higher than that of the damping and nonlinear terms. Therefore, for a periodic type of excitation, one has

$$\ddot{q}(T) + 2\beta\epsilon\dot{q}(T) + \omega^2 q(T) + \alpha\epsilon q^3(T) = 2\tilde{F}\cos(\Omega T), \tag{49}$$

where Ω is the excitation frequency.

On the other hand, the following multiple-timescale summation is considered for q:

$$q\,(T) = q_0\,(T_0, T_1) + \epsilon q_1\,(T_0, T_1)\,, \tag{50}$$

in which $T_0 = T$ and $T_1 = \epsilon T$. Inserting Eq. (50) into Eq. (49) yields

$$\begin{cases} O\left(\epsilon^0\right): \ \mathcal{D}_0^2 q_0 + \omega^2 q_0 = 2\tilde{F}\cos\left(\Omega T_0\right), \\ O\left(\epsilon^1\right): \ \mathcal{D}_0^2 q_1 + \omega^2 q_1 = -2\mathcal{D}_0\mathcal{D}_1 q_0 - 2\beta\mathcal{D}_0 q_0 - \alpha q_0^3, \end{cases} \tag{51}$$

where $\mathcal{D}_i^j = \frac{\mathrm{d}^j}{\mathrm{d}T_i^j}$ are time derivatives.

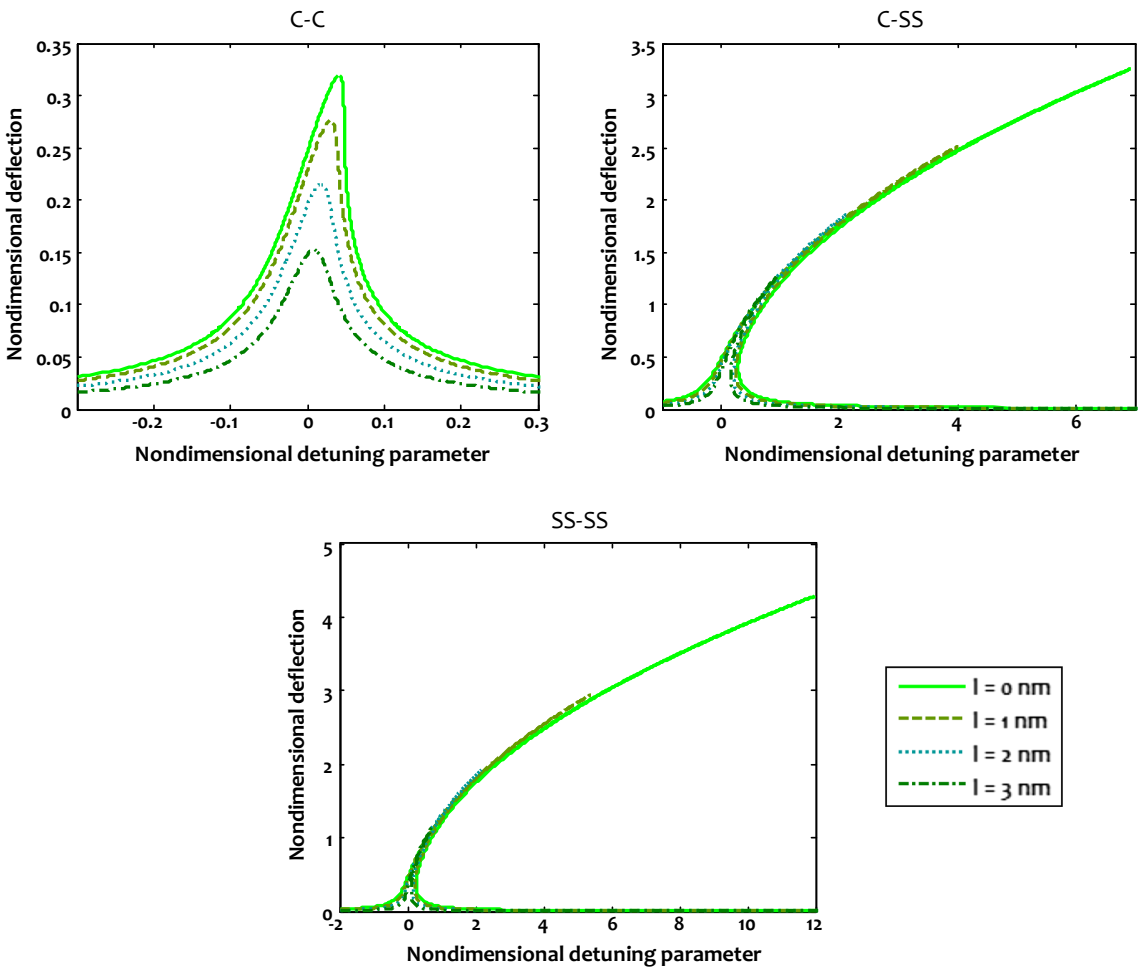

Fig. 6 Size-dependent frequency response of the micro-/nano-beam under superharmonic excitation corresponding to different strain gradient parameters and boundary conditions ($\mu = 0$ nm)

Based upon the first relation of Eq. (51), one has

$$q_0 = \mathcal{A}(T_1)\, e^{i\omega T_0} + \Delta e^{i\omega T_0} + \mathcal{B}(T_1)\, e^{i\omega T_0}, \tag{52}$$

in which $\mathcal{B}(T_1)$ stands for the complex conjugate part of the expression, and

$$\Delta = \frac{\tilde{F}}{\omega^2 - \Omega^2}. \tag{53}$$

Afterward, substitution of Eq. (52) into the second relation of Eq. (51) yields

$$\begin{aligned} \mathcal{D}_0^2 q_1 + \omega^2 q_1 = &-\left[2i\omega_0\left(\frac{\mathrm{d}\mathcal{A}}{\mathrm{d}T_1} + \mathcal{A}\beta\right) + 6\alpha\mathcal{A}\Delta^2 + 3\alpha\mathcal{A}^2\mathcal{B}\right] e^{i\omega T_0} \\ &-\alpha\left\{\mathcal{A}^3 e^{3i\omega T_0} + \Delta^3 e^{3i\omega T_0} + 3\mathcal{A}^2\Delta e^{i(2\omega+\Omega)T_0} + 3\Delta\left(\frac{\mathrm{d}\mathcal{A}}{\mathrm{d}T_1}\right)^2 e^{i(\Omega-2\omega)T_0}\right. \\ &\left.+3\mathcal{A}\Delta^2 e^{i(\omega+2\Omega)T_0} + 3\mathcal{A}\Delta^2 e^{i(\omega-2\Omega)T_0} - \Delta\left[2i\beta\Omega + 3\alpha\Delta^2 + 6\alpha\mathcal{A}\left(\frac{\mathrm{d}\mathcal{A}}{\mathrm{d}T_1}\right)\right] e^{i\omega T_0}\right\} \\ &+\cdots \end{aligned} \tag{54}$$

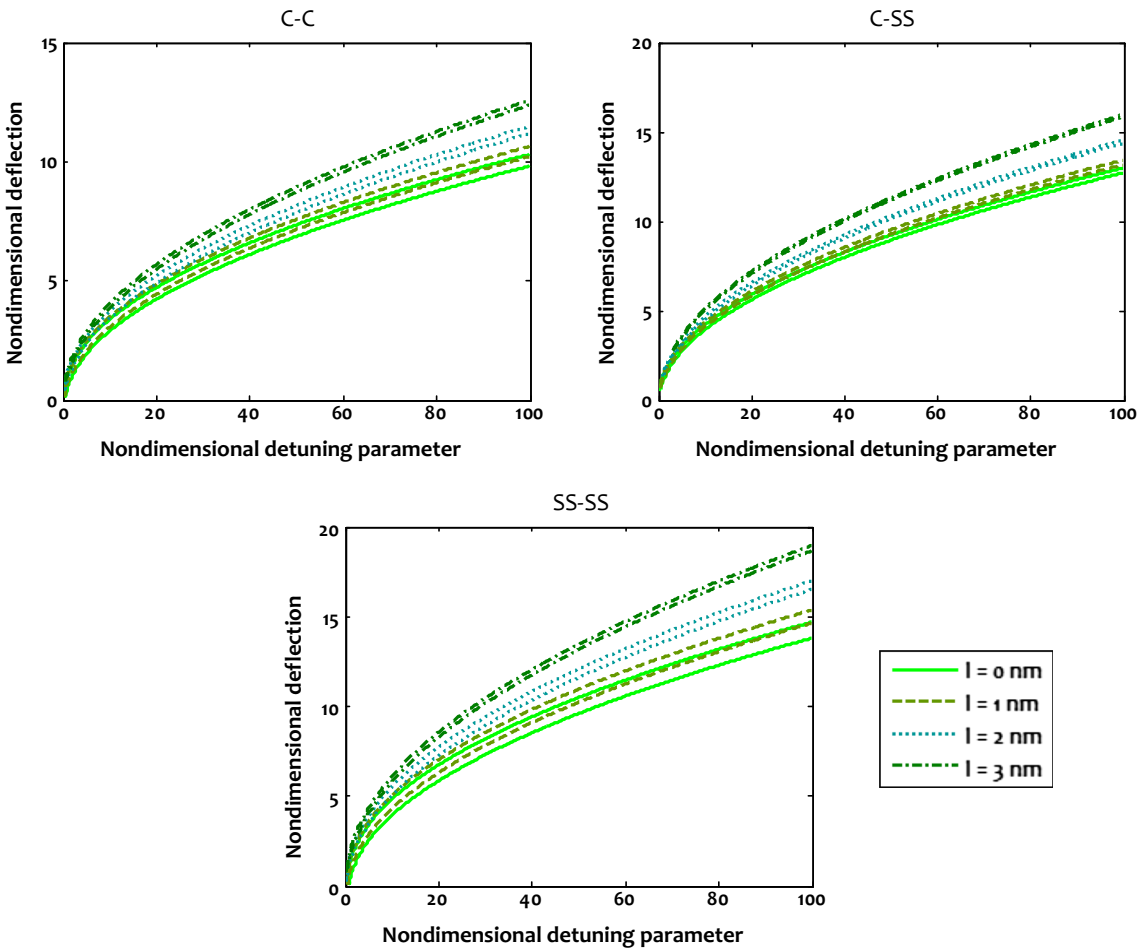

Fig. 7 Size-dependent frequency response of the micro-/nano-beam under subharmonic excitation corresponding to different strain gradient parameters and boundary conditions ($\mu = 0$ nm)

4.1 Superharmonic excitation

Within the range of superharmonic excitation, it can be written

$$3\Omega = \omega + \epsilon\Gamma, \tag{55}$$

where Γ represents the detuning parameter. By setting the secular and small divisor terms equal to zero, one has

$$2i\omega_0\left(\frac{\mathrm{d}\mathcal{A}}{\mathrm{d}T_1} + \mathcal{A}\beta\right) + 6\alpha\mathcal{A}\Delta^2 + 3\alpha\mathcal{A}^2\mathcal{B} + \alpha\Delta^3 e^{3i\Gamma T_1} = 0. \tag{56}$$

For $\mathcal{A}(T_1)$, a polar function is considered as follows:

$$\mathcal{A}(T_1) = \frac{1}{2}a(T_1)\, e^{i\xi(T_1)}. \tag{57}$$

Through substitution of Eq. (57) into Eq. (56), each of the real and imaginary parts gives

$$\frac{\mathrm{d}a}{\mathrm{d}T_1} = -\beta a + \frac{1}{2}\frac{\alpha\Delta^3}{\omega}\sin(\Gamma T_1 - \xi), \tag{58a}$$

$$a\frac{\mathrm{d}\xi}{\mathrm{d}T_1} = \frac{3\alpha a}{\omega}\left(\Delta^2 + \frac{a^2}{8}\right) + \frac{\alpha\Delta^3}{\omega}\cos(\Gamma T_1 - \xi). \tag{58b}$$

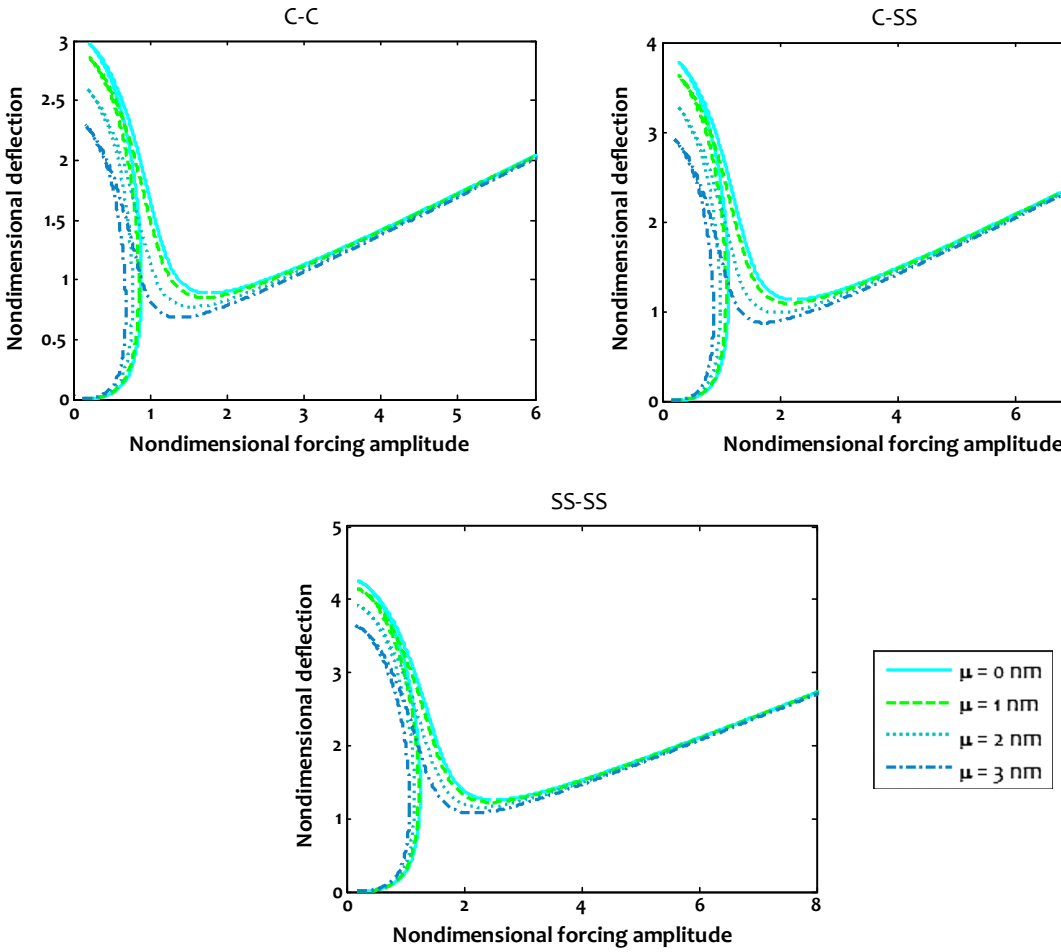

Fig. 8 Size-dependent amplitude response of the micro-/nano-beam under superharmonic excitation corresponding to different nonlocal parameters and boundary conditions ($l = 0$ nm, $\Gamma = 30$)

By setting the derivative terms on the left side of Eq. (58) equal to zero, the steady-state solution can be captured as

$$\left[\beta^2+\left(\Gamma-\frac{3\alpha\Delta^2}{\omega}-\frac{3\alpha a^2}{8\omega}\right)^2\right]a^2=\frac{\alpha^2\Delta^6}{\omega^2}. \tag{59}$$

Therefore, the size-dependent frequency response associated with the superharmonic excitation of a micro-/nano-beam can be given as

$$\Gamma=\frac{3\alpha\Delta^2}{\omega}+\frac{3\alpha a^2}{8\omega}\pm\sqrt{\frac{\alpha^2\Delta^6}{a^2\omega^2}-\beta^2}. \tag{60}$$

Equation (39) can be rewritten as

$$\left(\beta^2+\Gamma^2+\frac{9\alpha^2\Delta^4}{\omega^2}+\frac{9\alpha^2a^4}{64\omega^2}-\frac{6\alpha\Delta^2\Gamma}{\omega}-\frac{3\alpha a^2\Gamma}{4\omega}+\frac{9\alpha^2a^2\Delta^2}{4\omega^2}\right)a^2=\frac{\alpha^2\Delta^6}{\omega^2}. \tag{61}$$

As a consequence, one gets

$$\varsigma_1\Delta^6+\varsigma_2\Delta^4+\varsigma_3\Delta^2+\varsigma_4=0, \tag{62}$$

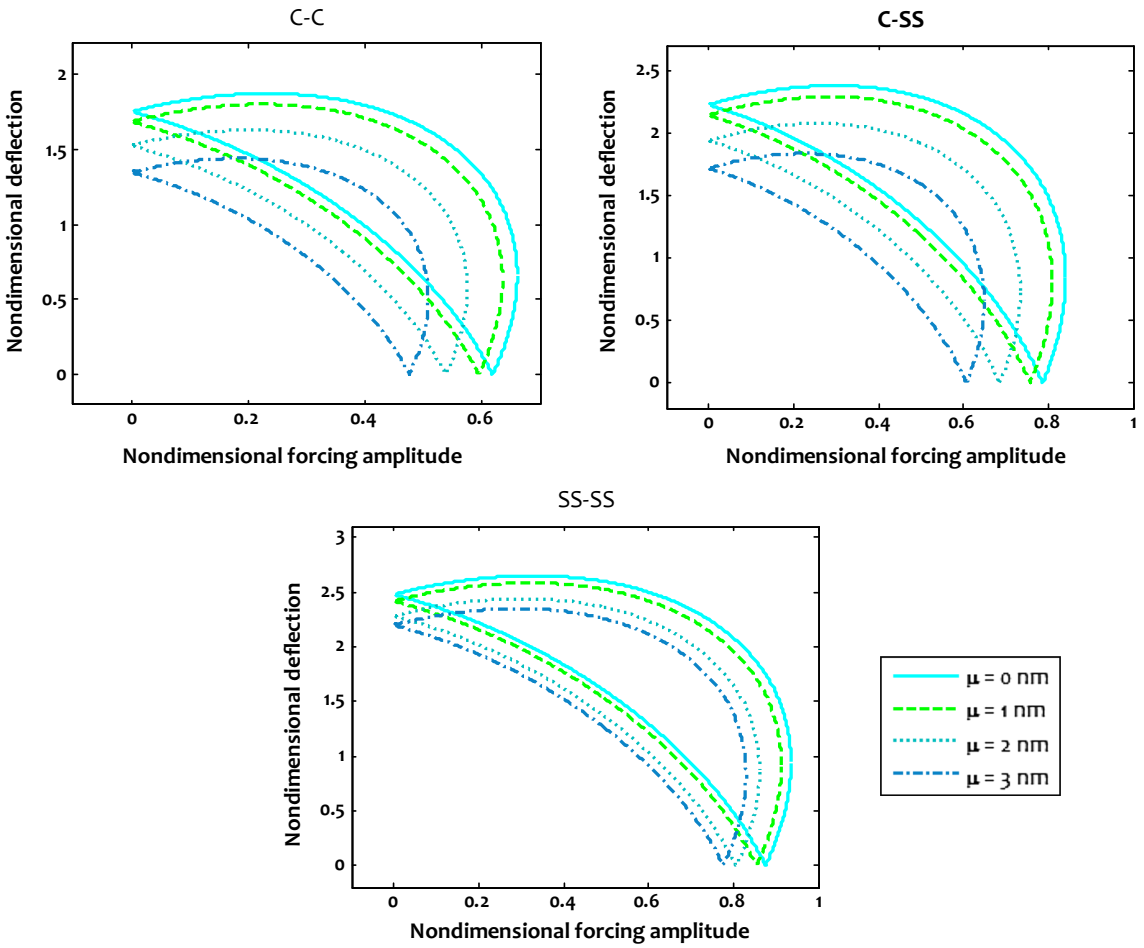

Fig. 9 Size-dependent amplitude response of the micro-/nano-beam under subharmonic excitation corresponding to different nonlocal parameters and boundary conditions ($l=0\,\text{nm}$, $\Gamma=30$)

in which

$$\varsigma_1 = \frac{\alpha^2}{\omega^2}, \quad \varsigma_2 = -\frac{9\alpha^2 a^2}{\omega^2}, \quad \varsigma_3 = \frac{6\alpha\Gamma a^2}{\omega} - \frac{9\alpha^2 a^4}{4\omega^2},$$
$$\varsigma_4 = -\left(\beta^2 + \Gamma^2 + \frac{9\alpha^2 a^4}{64\omega^2} - \frac{3\alpha a^2 \Gamma}{4\omega}\right) a^2. \tag{63}$$

The solution of Eq. (62) represents the size-dependent amplitude response related to the superharmonic excitation of a micro-/nano-beam.

4.2 Subharmonic excitation

Within the range of subharmonic excitation, it can be written

$$\Omega = 3\omega + \epsilon\Gamma. \tag{64}$$

After that, in accordance with Eq. (54), the secular and small divisor terms are set equal to zero as follows:

$$2i\omega_0\left(\frac{\mathrm{d}\mathcal{A}}{\mathrm{d}T_1} + \mathcal{A}\beta\right) + 6\alpha\mathcal{A}\Delta^2 + 3\alpha\mathcal{A}^2\mathcal{B} + 3\Delta\left(\frac{\mathrm{d}\mathcal{A}}{\mathrm{d}T_1}\right)^2 e^{i\Gamma T_1} = 0. \tag{65}$$

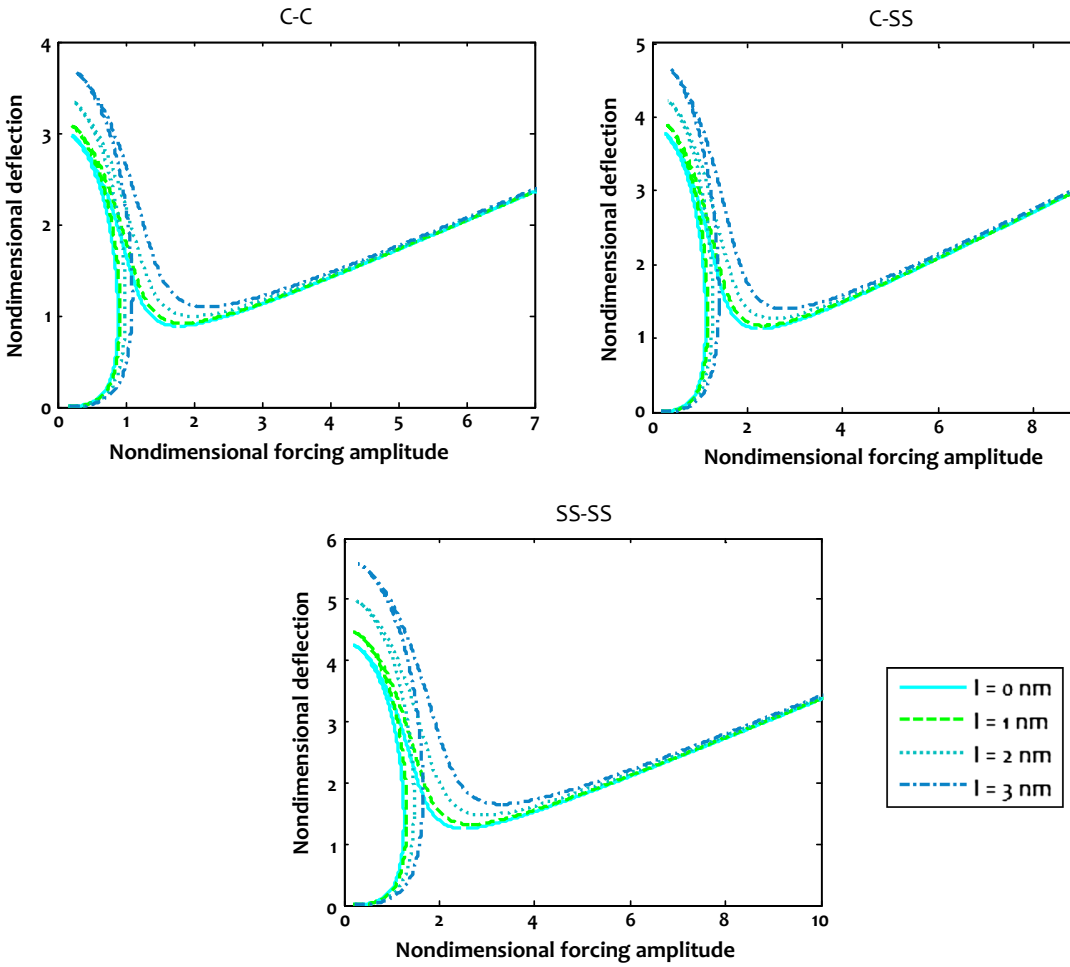

Fig. 10 Size-dependent amplitude response of the micro-/nano-beam under superharmonic excitation corresponding to different strain gradient parameters and boundary conditions ($\mu = 0$ nm, $\Gamma = 30$)

By Eq. (57), a polar function is introduced for $\mathcal{A}(T_1)$, so one has

$$\frac{\mathrm{d}a}{\mathrm{d}T_1} = -\beta a - \frac{3}{4}\frac{\alpha a^2 \Delta}{\omega}\sin\left(\Gamma T_1 - 3\xi\right), \tag{66a}$$

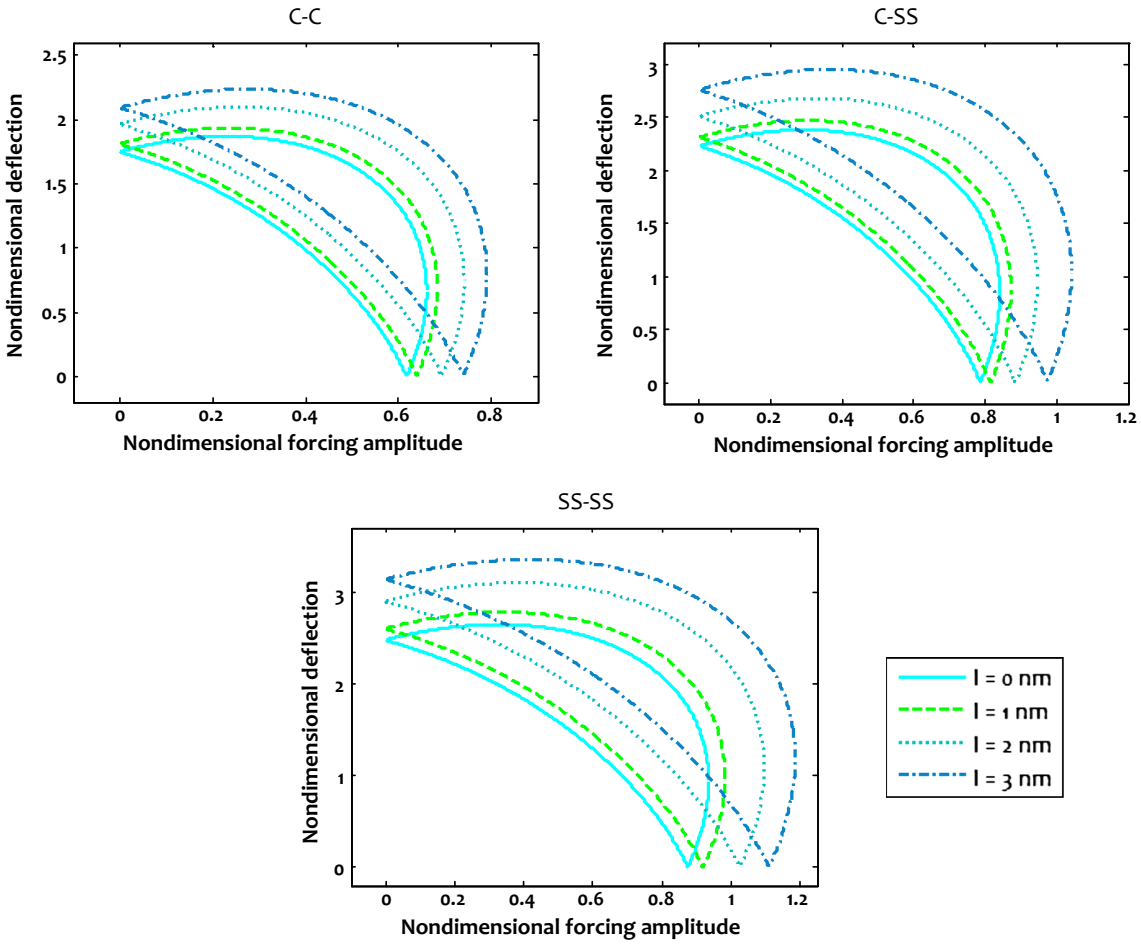

Fig. 11 Size-dependent amplitude response of the micro-/nano-beam under subharmonic excitation corresponding to different strain gradient parameters and boundary conditions ($\mu = 0\,\mathrm{nm}$, $\Gamma = 30$)

Table 1 Nondimensional natural frequencies (ω_{L}) of a micro-/nano-beam corresponding to various small-scale parameters and boundary conditions ($\ell/r = 10$)

Small-scale parameters (nm)	C–C boundary conditions	C–SS boundary conditions	SS–SS boundary conditions
$\mu = 0, l = 0$	0.6342	0.4531	0.2900
$\mu = 0.5, l = 0$	0.6329 (−0.205%)	0.4519 (−0.265%)	0.2891 (−0.310%)
$\mu = 1, l = 0$	0.6292 (−0.788%)	0.4487 (−0.971%)	0.2865 (−1.207%)
$\mu = 1.5, l = 0$	0.6225 (−1.845%)	0.4431 (−2.207%)	0.2823 (−2.655%)
$\mu = 2, l = 0$	0.6137 (−3.232%)	0.4359 (−3.796%)	0.2767 (−4.486%)
$\mu = 2.5, l = 0$	0.6039 (−4.778%)	0.4266 (−5.849%)	0.2696 (−7.034%)
$\mu = 3, l = 0$	0.5918 (−6.686%)	0.4170 (−7.967%)	0.2623 (−9.552%)
$\mu = 0, l = 0.5$	0.6355 (+0.205%)	0.4542 (+0.243%)	0.2909 (+0.310%)
$\mu = 0, l = 1$	0.6395 (+0.836%)	0.4576 (+0.993%)	0.2935 (+1.207%)
$\mu = 0, l = 1.5$	0.6461 (+1.883%)	0.4621 (+1.986%)	0.2979 (+2.724%)
$\mu = 0, l = 2$	0.6569 (+3.358%)	0.4705 (+3.840%)	0.3040 (+4.828%)
$\mu = 0, l = 2.5$	0.6665 (+5.093%)	0.4818 (+6.334%)	0.3115 (+7.414%)
$\mu = 0, l = 3$	0.6803 (+7.269%)	0.4926 (+8.718%)	0.3206 (+10.551%)

$$a\frac{\mathrm{d}\xi}{\mathrm{d}T_1}=\frac{3\alpha a}{\omega}\left(\Delta^2+\frac{a^2}{8}\right)+\frac{3}{4}\frac{\alpha a^2\Delta}{\omega}\cos\left(\Gamma T_1-3\xi\right). \tag{66b}$$

To capture the steady-state solution, the derivative terms on the left side of Eq. (66) are set to be zero. As a result,

$$9\beta^2+\left(\Gamma-\frac{9\alpha\Delta^2}{\omega}-\frac{9\alpha a^2}{8\omega}\right)^2=\frac{81\alpha^2a^2\Delta^2}{16\omega^2}. \tag{67}$$

Thus, the size-dependent frequency response associated with the subharmonic excitation of a micro-/nano-beam can be presented as

$$\Gamma=\frac{9\alpha\Delta^2}{\omega}+\frac{9\alpha a^2}{8\omega}\pm\sqrt{\frac{81\alpha^2a^2\Delta^2}{16\omega^2}-9\beta^2}. \tag{68}$$

Additionally, Eq. (67) can be rewritten as

$$\left(9\beta^2+\Gamma^2+\frac{81\alpha^2\Delta^4}{\omega^2}+\frac{81\alpha^2a^4}{64\omega^2}-\frac{18\alpha\Delta^2\Gamma}{\omega}-\frac{9\alpha a^2\Gamma}{4\omega}+\frac{81\alpha^2a^2\Delta^2}{4\omega^2}\right)=\frac{81\alpha^2a^2\Delta^2}{16\omega^2}. \tag{69}$$

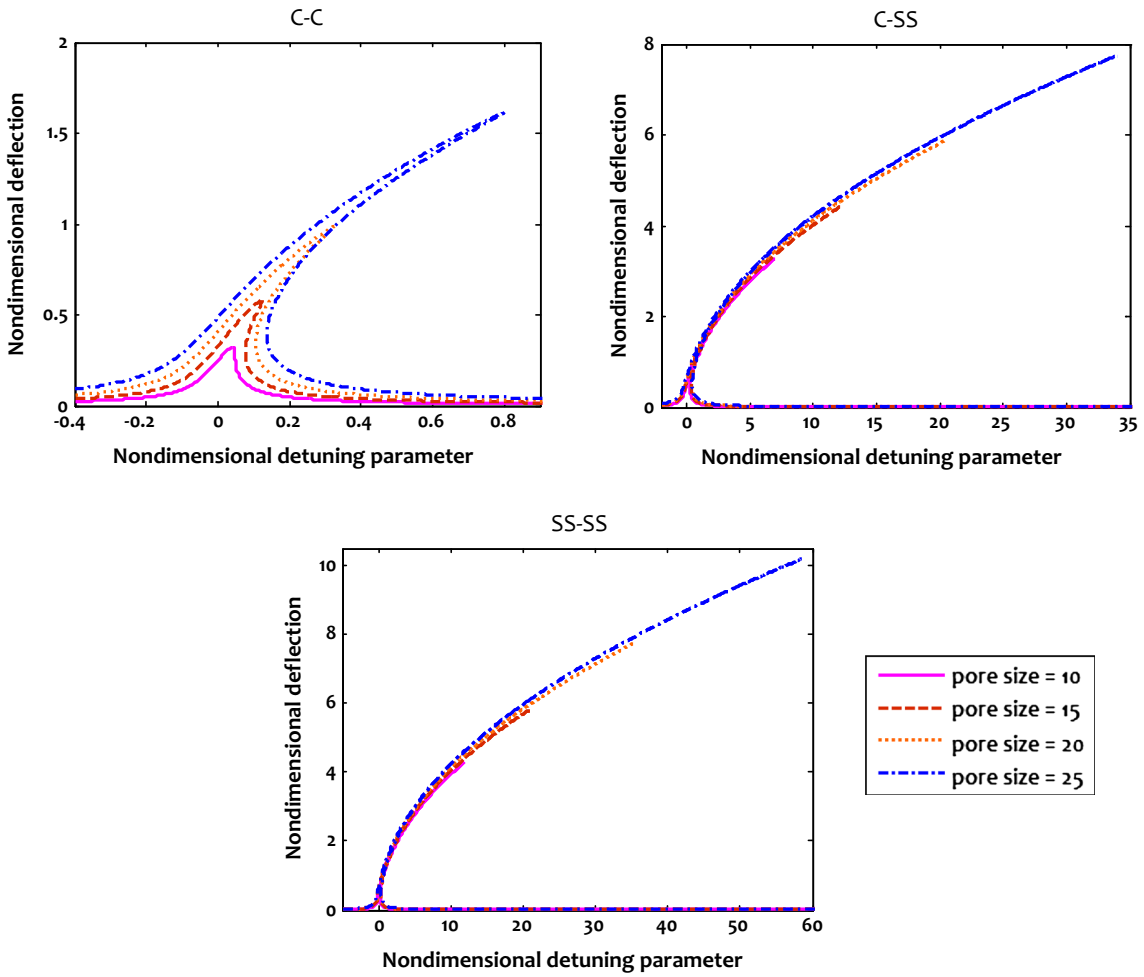

Fig. 12 Influence of pore size on the size-dependent frequency response of a micro-/nano-beam made of nano-porous biomaterial under superharmonic excitation ($\mu = l = 1$ nm)

So, one obtains

$$\mathcal{S}_1\Delta^4 + \mathcal{S}_2\Delta^2 + \mathcal{S}_3 = 0, \tag{70}$$

where

$$\mathcal{S}_1 = \frac{81\alpha^2}{\omega^2}, \quad \mathcal{S}_2 = \frac{243\alpha^2 a^2}{16\omega^2} - \frac{18\alpha\Gamma}{\omega},$$
$$\mathcal{S}_3 = 9\beta^2 + \Gamma^2 + \frac{81\alpha^2 a^4}{64\omega^2} - \frac{9\alpha a^2\Gamma}{4\omega}. \tag{71}$$

The solution of Eq. (70) yields the size-dependent amplitude response associated with the subharmonic excitation of a micro-/nano-beam.

5 Numerical results and discussion

Now, based upon the captured mechanical properties of the nano-porous biomaterials as functions of pore size, the nonlinear secondary resonance of a micro-/nano-beam made of this material under subharmonic and superharmonic excitations is numerically depicted corresponding to different pore sizes. For the micro-/nano-beam, it is assumed that $b = h = 2$ nm, $L/h = 20$, $\tilde{F} = 0.1$ and $\eta = 0.5$.

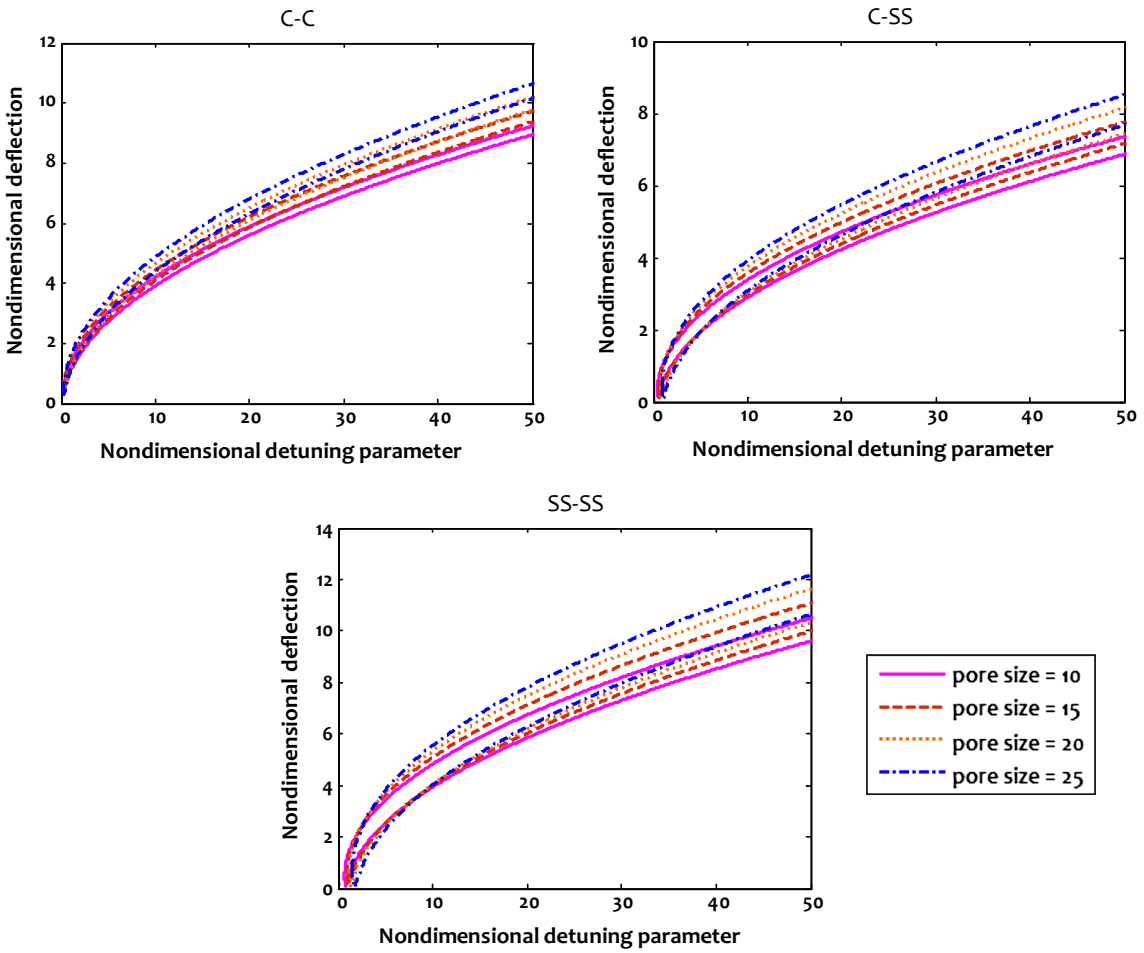

Fig. 13 Influence of pore size on the size-dependent frequency response of a micro-/nano-beam made of nano-porous biomaterial under subharmonic excitation ($\mu = l = 1$ nm)

Figures 4 and 5 illustrate, respectively, the nonlocal size effect on the frequency response of a micro-/nano-beam with pore size of $\ell/r = 10$ under superharmonic and subharmonic excitations. It is revealed that in the case of superharmonic excitation, the jump phenomenon occurs and the nonlocality causes an enhancement of both nonlinear hardening spring-type behavior and the height of limit point bifurcations. In the case of subharmonic excitation, there are two branches including the high-frequency and low-frequency solutions. By taking the nonlocality into consideration, the gap between these branches increases.

In Figs. 6 and 7, the strain gradient size dependency on the frequency response of a micro-/nano-beam with pore size of $\ell/r = 10$ is shown corresponding to the superharmonic and subharmonic excitations, respectively. It can be seen that in the case of superharmonic excitation, the strain gradient size effect leads to a reduction in the nonlinear hardening spring-type behavior as well as the height of limit point bifurcations. For the subharmonic case of the study, the strain gradient size dependency causes a decrease in the gap between the two branches associated with the high-frequency and low-frequency solutions.

The influence of nonlocality on the amplitude response of a micro-/nano-beam with pore size of $\ell/r = 10$ is depicted in Figs. 8 and 9 corresponding to, respectively, the superharmonic and subharmonic excitations. It is observed that in the superharmonic case, both types of upward jump and downward jump exist. By taking the nonlocal size effect, the maximum amplitude of the response related to the downward jump decreases, so through a reduction in the amplitude of the excitation, the amplitude of the responses vanishes less rapidly. For the subharmonic case, it is indicated that the micro-/nano-beam is excited within a specific range of the amplitude of the excitation. The width of this range decreases by taking the nonlocal size effect into account.

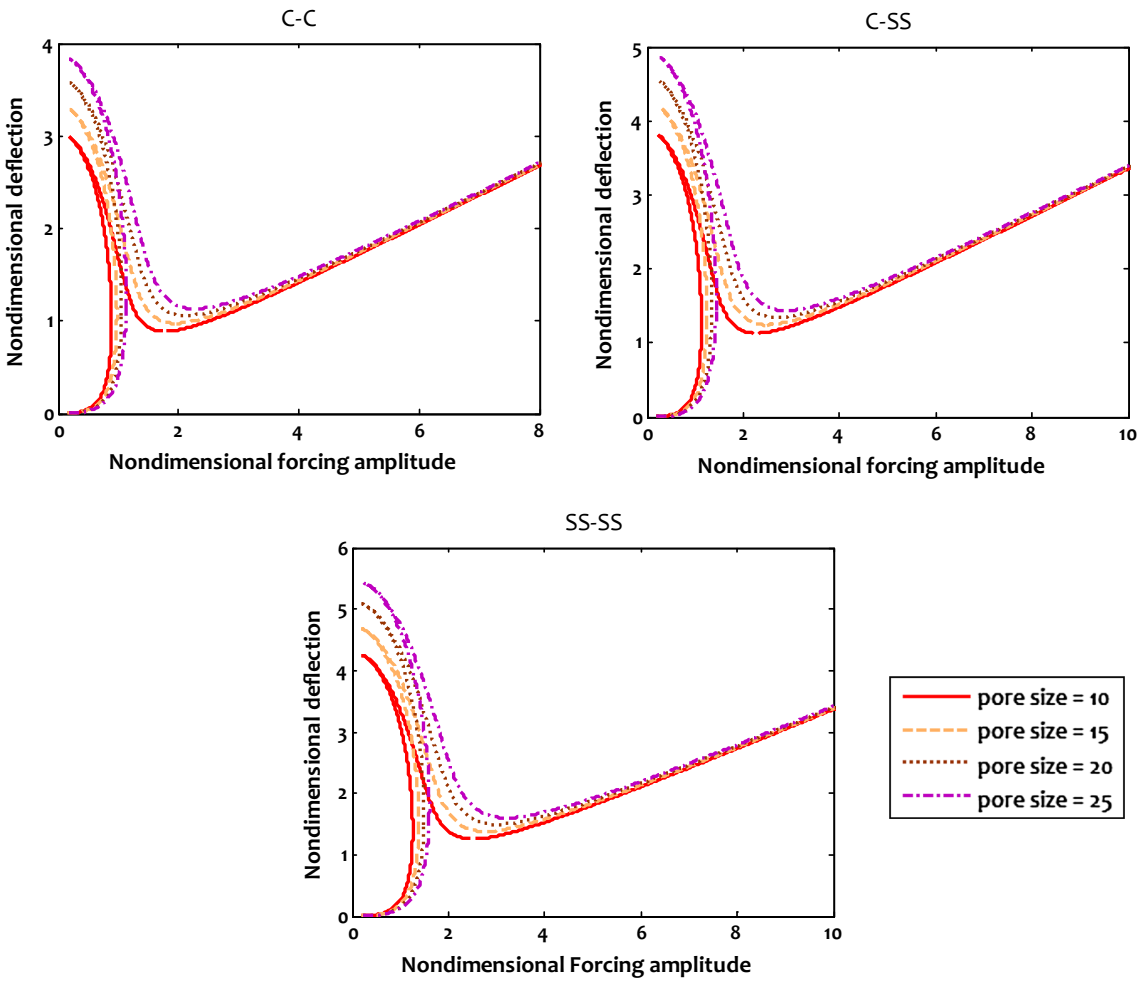

Fig. 14 Influence of pore size on the size-dependent amplitude response of a micro-/nano-beam made of nano-porous biomaterial under superharmonic excitation ($\mu = l = 1$ nm, $\Gamma = 30$)

Figures 10 and 11 display, respectively, the strain gradient size effect on the amplitude response of a micro-/nano-beam with pore size of $\ell/r = 10$ subjected to superharmonic and subharmonic excitations. It is found that for the superharmonic excitation, the strain gradient size dependency leads to an increase in the maximum amplitude of the response related to the downward jump. As a result, by decreasing the amplitude of the excitation, the amplitude of the responses vanishes more rapidly. Also, in the case of the subharmonic excitation, the amplitude range of the excitation within which the micro-/nano-beam is excited becomes wider due to the strain gradient size effect.

In order to compare the significance of the two different size dependencies, in Table 1, the influences of the nonlocality and strain gradient size dependency on the natural frequency of a micro-/nano-beam made of nano-porous biomaterial with pore size of $\ell/r = 10$ are represented corresponding to different boundary conditions. The percentages given in the parentheses indicate the difference of the size-dependent natural frequency with its classical counterpart. It can be found that both nonlocality and strain gradient size dependency have the minimum and maximum influences on the natural frequency of the micro-/nano-beam with clamped and simply supported edge supports, respectively. Moreover, by increasing the values of small-scale parameters, the influence of the strain gradient size effect is stronger than that of the nonlocal one.

In Figs. 12 and 13, the frequency response of a micro-/nano-beam made of the nano-porous biomaterial with various pores sizes is demonstrated corresponding to the superharmonic and subharmonic excitations, respectively. It can be observed that in the superharmonic case, increasing the pore size leads to an enhancement of the nonlinear hardening spring-type behavior and the height of limit point bifurcations. In the subharmonic case, the higher pore size causes an increase in the gap between the two branches related to the high-frequency and low-frequency solutions.

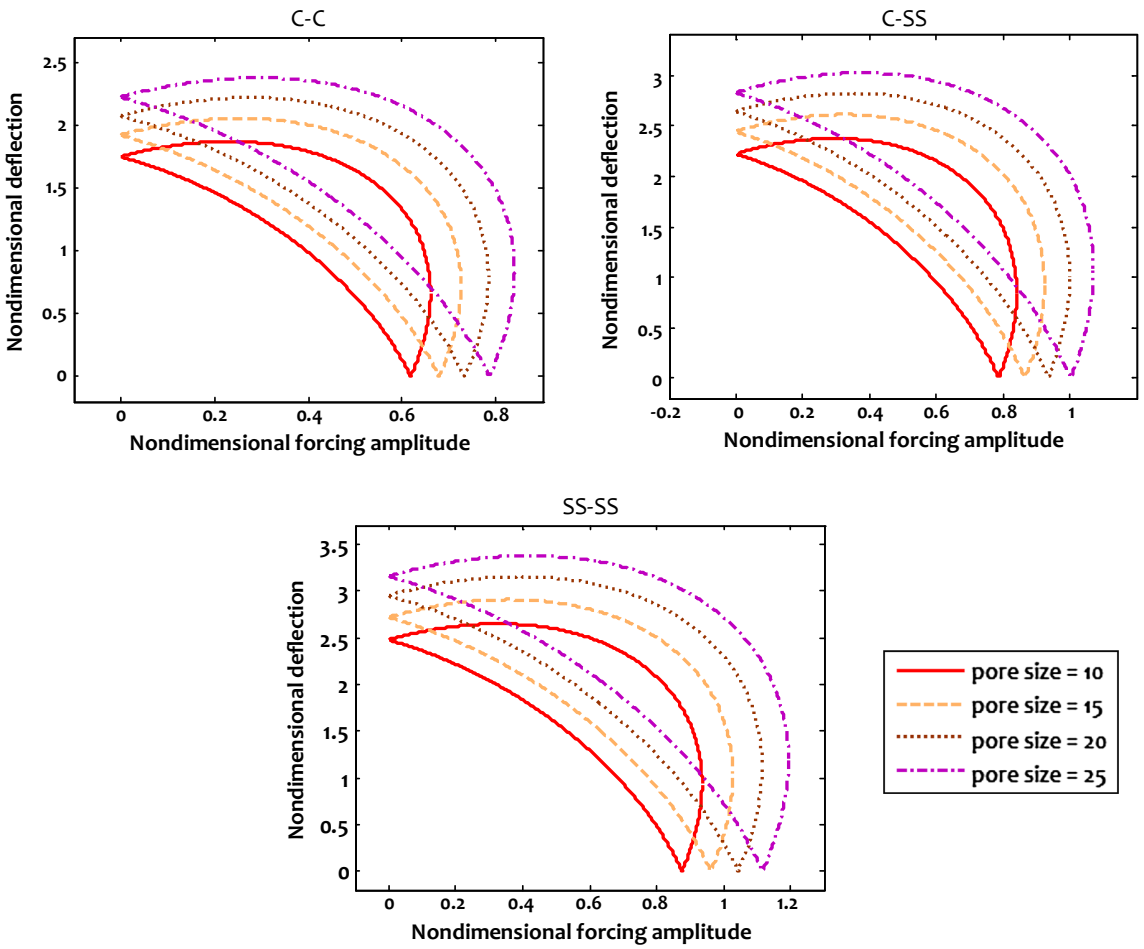

Fig. 15 Influence of pore size on the size-dependent amplitude response of a micro-/nano-beam made of nano-porous biomaterial under subharmonic excitation ($\mu = l = 1$ nm, $\Gamma = 30$)

The influence of pore size on the amplitude response of a micro-/nano-beam made of the nano-porous biomaterial is plotted in Figs. 14 and 15 for the superharmonic and subharmonic excitations, respectively. In the superharmonic case, it can be found that by increasing the pore size, the maximum amplitude of the response related to the downward jump is enhanced so a reduction in the amplitude of the excitation leads to the vanishing of the amplitude of the responses more rapidly. In the subharmonic case, it is revealed that increasing the pore size causes the widening of the range of the amplitude of the excitation within which the micro-/nano-beam is excited.

6 Concluding remarks

The objective of the current study was to analyze the size-dependent nonlinear secondary resonance of a micro-/nano-beam made of nano-porous biomaterials. On the basis of a refined truncated cubic unit cell, analytical expressions for the mechanical properties of the nano-porous biomaterial were obtained as functions of pore size. Subsequently, the Galerkin technique together with the multiple-timescale method was employed to predict the size-dependent frequency response and amplitude response of the micro-/nano-beam with different pore sizes and end supports corresponding to the subharmonic and superharmonic excitations.

It was demonstrated that in the case of superharmonic excitation, the jump phenomenon occurs and the nonlocality and strain gradient size dependencies cause, respectively, an increase and decrease in both nonlinear hardening spring-type behavior and the height of limit point bifurcations. In the case of subharmonic excitation, there is two branches including the high-frequency and low-frequency solutions. By taking the nonlocal and strain gradient size effects into consideration, the gap between these branches increases and decreases, respectively. Additionally, it was seen that both nonlocality and strain gradient size dependency have the minimum and maximum influences on the natural frequency of the micro-/nano-beam with clamped and simply supported edge supports, respectively. Furthermore, it was observed that in the superharmonic case, by increasing the pore size, the maximum amplitude of the response related to the downward jump enhances, so a reduction in the amplitude of the excitation leads to the vanishing of the amplitude of the responses more rapidly. In the subharmonic case, it was found that increasing the pore size causes a widening of the range of the amplitude of the excitation within which the micro-/nano-beam is excited.

Appendix A

$$\mathcal{K}_{11}=\frac{2\bar{A}\bar{E}}{\ell},\quad \mathcal{K}_{21}=-\frac{2\bar{A}\bar{E}}{\ell},\quad \mathcal{K}_{31}=\mathcal{K}_{41}=\mathcal{K}_{51}=\mathcal{K}_{61}=0$$

$$\mathcal{K}_{12}=-\frac{2\bar{A}\bar{E}}{\ell},\quad \mathcal{K}_{42}=\mathcal{K}_{62}=0$$

$$\mathcal{K}_{22}=\frac{4\bar{A}\bar{E}}{\ell}+\frac{1}{\frac{\ell^3}{24\bar{E}\bar{I}}+\frac{3\ell}{10\bar{G}\bar{A}}+\frac{3}{5\bar{G}\bar{A}}\left(\frac{\left(1+\frac{p\ell}{2}\right)\cosh(p\ell)-\left(1+\frac{p\ell}{2}\right)\sinh(p\ell)-1}{p}\right)}$$

$$\mathcal{K}_{32}=-\frac{2\bar{A}\bar{E}}{\ell}-\frac{1}{\frac{\ell^3}{24\bar{E}\bar{I}}+\frac{3\ell}{10\bar{G}\bar{A}}+\frac{3}{5\bar{G}\bar{A}}\left(\frac{\left(1+\frac{p\ell}{2}\right)\cosh(p\ell)-\left(1+\frac{p\ell}{2}\right)\sinh(p\ell)-1}{p}\right)}$$

$$\mathcal{K}_{52}=-\frac{2\bar{A}\bar{E}}{\ell}+\frac{1}{\frac{\ell^3}{24\bar{E}\bar{I}}+\frac{3\ell}{10\bar{G}\bar{A}}+\frac{3}{5\bar{G}\bar{A}}\left(\frac{\left(1+\frac{p\ell}{2}\right)\cosh(p\ell)-\left(1+\frac{p\ell}{2}\right)\sinh(p\ell)-1}{p}\right)}$$

$$\mathcal{K}_{13}=\mathcal{K}_{53}=\mathcal{K}_{63}=0$$

$$\mathcal{K}_{23}=\mathcal{K}_{43}=\frac{2\bar{A}\bar{E}}{\ell}-\frac{1}{\frac{\ell^3}{24\bar{E}\bar{I}}+\frac{3\ell}{10\bar{G}\bar{A}}+\frac{3}{5\bar{G}\bar{A}}\left(\frac{\left(1+\frac{p\ell}{2}\right)\cosh(p\ell)-\left(1+\frac{p\ell}{2}\right)\sinh(p\ell)-1}{p}\right)}$$

$$\mathcal{K}_{33}=\frac{4\bar{A}\bar{E}}{\ell}+\frac{1}{\frac{\ell^3}{48\bar{E}\bar{I}}+\frac{3\ell}{20\bar{G}\bar{A}}+\frac{3}{10\bar{G}\bar{A}}\left(\frac{\left(1+\frac{p\ell}{2}\right)\cosh(p\ell)-\left(1+\frac{p\ell}{2}\right)\sinh(p\ell)-1}{p}\right)}$$

$$\mathcal{K}_{14}=\mathcal{K}_{24}=\mathcal{K}_{64}=0$$

$$\mathcal{K}_{34}=-\frac{2\bar{A}\bar{E}}{\ell}-\frac{1}{\frac{\ell^3}{24\bar{E}\bar{I}}+\frac{3\ell}{10\bar{G}\bar{A}}+\frac{3}{5\bar{G}\bar{A}}\left(\frac{\left(1+\frac{p\ell}{2}\right)\cosh(p\ell)-\left(1+\frac{p\ell}{2}\right)\sinh(p\ell)-1}{p}\right)}$$

$$\mathcal{K}_{44}=\frac{4\bar{A}\bar{E}}{\ell}+\frac{1}{\frac{\ell^3}{24\bar{E}\bar{I}}+\frac{3\ell}{10\bar{G}\bar{A}}+\frac{3}{5\bar{G}\bar{A}}\left(\frac{\left(1+\frac{p\ell}{2}\right)\cosh(p\ell)-\left(1+\frac{p\ell}{2}\right)\sinh(p\ell)-1}{p}\right)}$$

$$\mathcal{K}_{54}=\frac{4\bar{A}\bar{E}}{\ell}+\frac{1}{\frac{\ell^3}{24\bar{E}\bar{I}}+\frac{3\ell}{10\bar{G}\bar{A}}+\frac{3}{5\bar{G}\bar{A}}\left(\frac{\left(1+\frac{p\ell}{2}\right)\cosh(p\ell)-\left(1+\frac{p\ell}{2}\right)\sinh(p\ell)-1}{p}\right)}$$

$$\mathcal{K}_{15}=\mathcal{K}_{35}=0$$

$$\mathcal{K}_{25}=-\frac{2\bar{A}\bar{E}}{\ell}+\frac{1}{\frac{\ell^3}{24\bar{E}\bar{I}}+\frac{3\ell}{10\bar{G}\bar{A}}+\frac{3}{5\bar{G}\bar{A}}\left(\frac{\left(1+\frac{p\ell}{2}\right)\cosh(p\ell)-\left(1+\frac{p\ell}{2}\right)\sinh(p\ell)-1}{p}\right)}$$

$$\mathcal{K}_{45}=\frac{2\bar{A}\bar{E}}{\ell}-\frac{1}{\frac{\ell^3}{24\bar{E}\bar{I}}+\frac{3\ell}{10\bar{G}\bar{A}}+\frac{3}{5\bar{G}\bar{A}}\left(\frac{\left(1+\frac{p\ell}{2}\right)\cosh(p\ell)-\left(1+\frac{p\ell}{2}\right)\sinh(p\ell)-1}{p}\right)}$$

$$\mathcal{K}_{55}=\frac{20\bar{A}\bar{E}}{\ell}+\frac{1}{\frac{\ell^3}{48\bar{E}\bar{I}}+\frac{3\ell}{20\bar{G}\bar{A}}+\frac{3}{10\bar{G}\bar{A}}\left(\frac{\left(1+\frac{p\ell}{2}\right)\cosh(p\ell)-\left(1+\frac{p\ell}{2}\right)\sinh(p\ell)-1}{p}\right)}$$

$$\mathcal{K}_{65}=-\frac{8\bar{A}\bar{E}}{\ell},\quad \mathcal{K}_{16}=\mathcal{K}_{26}=\mathcal{K}_{36}=\mathcal{K}_{46}=0,\quad \mathcal{K}_{56}=-\frac{8\bar{A}\bar{E}}{\ell},\quad \mathcal{K}_{66}=\frac{8\bar{A}\bar{E}}{\ell}$$

References

1. Sahmani, S., Shahali, M., Khandan, A., Saber-Samandari, S., Aghdam, M.M.: Analytical and experimental analyses for mechanical and biological characteristics of novel nanoclay bio-nanocomposite scaffolds fabricated via space holder technique. Appl. Clay Sci. **165**, 112–123 (2018)
2. Sahmani, S., Saber-Samandari, S., Shahali, M., Yekta, H.J., Aghadavoudi, F., Montazeran, A.H., Aghdam, M.M., Khandan, A.: Mechanical and biological performance of axially loaded novel bio-nanocomposite sandwich plate-type implant coated by biological polymer thin film. J Mech. Behav. Biomed. Mater. **88**, 238–250 (2018)
3. Sahmani, S., Saber-Samandari, S., Khandan, A., Aghdam, M.M.: Nonlinear resonance investigation of nanoclay based bio-nanocomposite scaffolds with enhanced properties for bone substitute applications. J. Alloys Compd. **773**, 636–653 (2019)
4. Safari, J., Zarnegar, Z.: Advanced drug delivery systems: nanotechnology of health design a review. J Saudi Chem. Soc. **18**, 85–99 (2014)
5. Usui, Y., Zerwekh, J.E., Vanharanta, H., Ashman, R.B., Mooney, V.: Different effects of mechanical vibration on bone ingrowth into porous hydroxyapatite and fracture healing in a rabbit model. J. Orthop. Res. **7**, 559–567 (1989)
6. Altintas, G.: Natural vibration behaviors of heterogeneous porous materials in micro scale. J. Vib. Control **20**, 1999–2005 (2014)
7. Eringen, A.C.: Linear theory of nonlocal elasticity and dispersion of plane waves. Int. J. Eng. Sci. **10**, 425–435 (1972)
8. Gurtin, M.E., Murdoch, A.I.: Surface stress in solids. Int. J. Solids Struct. **14**, 431–440 (1978)
9. Lam, D., Yang, F., Chong, A., Wang, J., Tong, P.: Experiments and theory in strain gradient elasticity. J. Mech. Phys. Solids **51**, 1477–1508 (2003)
10. Yang, F., Chong, A., Lam, D., Tong, P.: Couple stress based strain gradient theory for elasticity. Int. J. Solids Struct. **39**, 2731–2743 (2002)

11. Li, Y.S., Cai, Z.Y., Shi, S.Y.: Buckling and free vibration of magnetoelectroelastic nanoplate based on nonlocal theory. Compos. Struct. **111**, 522–529 (2014)
12. Daneshmand, F., Farokhi, H., Amabili, M.: A higher-order mathematical modeling for dynamic behavior of protein microtubule shell structures including shear deformation and small-scale effects. Math. Biosci. **252**, 67–82 (2014)
13. Fakhrabadi, M.M.S., Rastgoo, A., Ahmadian, M.T.: Non-linear behaviors of carbon nanotubes under electrostatic actuation based on strain gradient theory. Int. J. Non Linear Mech. **67**, 236–244 (2014)
14. Sahmani, S., Aghdam, M.M., Bahrami, M.: On the postbuckling behavior of geometrically imperfect cylindrical nanoshells subjected to radial compression including surface stress effects. Compos. Struct. **131**, 414–424 (2015)
15. Ghorbanpour Arani, A., Abdollahian, M., Jalaei, M.H.: Vibration of bioliquid-filled microtubules embedded in cytoplasm including surface effects using modified couple stress theory. J. Theor. Biol. **367**, 29–38 (2015)
16. Zhang, J., Meguid, S.A.: Effect of surface energy on the dynamic response and instability of fluid-conveying nanobeams. Eur. J. Mech. A/Solids **58**, 1–9 (2016)
17. Sahmani, S., Aghdam, M.M., Akbarzadeh, A.H.: Size-dependent buckling and postbuckling behavior of piezoelectric cylindrical nanoshells subjected to compression and electrical load. Mater. Des. **105**, 341–351 (2016)
18. Shaat, M., Abdelkefi, A.: Size dependent and micromechanical modeling of strain gradient-based nanoparticle composite plates with surface elasticity. Eur. J. Mech. A/Solids **58**, 54–68 (2016)
19. Sahmani, S., Aghdam, M.M., Bahrami, M.: Surface free energy effects on the postbuckling behavior of cylindrical shear deformable nanoshells under combined axial and radial compressions. Meccanica **52**, 1329–1352 (2017)
20. Sahmani, S., Aghdam, M.M., Bahrami, M.: An efficient size-dependent shear deformable shell model and molecular dynamics simulation for axial instability analysis of silicon nanoshells. J. Mol. Graph. Modell. **77**, 263–279 (2017)
21. Fernandez-Saez, J., Zaera, R.: Vibrations of Bernoulli–Euler beams using the two-phase nonlocal elasticity theory. Int. J. Eng. Sci. **119**, 232–248 (2017)
22. Sahmani, S., Aghdam, M.M., Bahrami, M.: Nonlinear buckling and postbuckling behavior of cylindrical shear deformable nanoshells subjected to radial compression including surface free energy effects. Acta Mech. Sol. Sin. **30**, 209–222 (2017)
23. Sahmani, S., Aghdam, M.M.: Nonlinear vibrations of pre-and post-buckled lipid supramolecular micro/nano-tubules via nonlocal strain gradient elasticity theory. J. Biomech. **65**, 49–60 (2017)
24. Shaat, M., Abdelkefi, A.: Material structure and size effects on the nonlinear dynamics of electrostatically-actuated nanobeams. Int. J. Non Linear Mech. **89**, 25–42 (2017)
25. Trinh, L.C., Vo, T.P., Thai, H.-T., Mantari, J.L.: Size-dependent behaviour of functionally graded sandwich microplates under mechanical and thermal loads. Compos. Part B Eng. **124**, 218–241 (2017)
26. Sahmani, S., Aghdam, M.M.: Imperfection sensitivity of the size-dependent postbuckling response of pressurized FGM nanoshells in thermal environments. Arch. Civil Mech. Eng. **17**, 623–638 (2017)
27. Sahmani, S., Fattahi, A.M.: Imperfection sensitivity of the size-dependent nonlinear instability of axially loaded FGM nanopanels in thermal environments. Acta Mech. **228**, 3789–3810 (2017)
28. Mercan, K., Civalek, O.: Buckling analysis of Silicon carbide nanotubes (SiCNTs) with surface effect and nonlocal elasticity using the method of HDQ. Compos. Part B Eng. **114**, 34–45 (2017)
29. Sahmani, S., Fattahi, A.M.: An anisotropic calibrated nonlocal plate model for biaxial instability analysis of 3D metallic carbon nanosheets using molecular dynamics simulations. Mater. Res. Expr. **4**, 065001 (2017)
30. Sahmani, S., Aghdam, M.M.: Size-dependent nonlinear bending of micro/nano-beams made of nanoporous biomaterials including a refined truncated cube cell. Phys. Lett. A **381**, 3818–3830 (2017)
31. Tadi beni, Y., Karimi Zeverdejani, M., Mehralian, F.: Buckling analysis of orthotropic protein microtubules under axial and radial compression based on couple stress theory. Math. Biosci. **292**, 18–29 (2017)
32. Nguyen, H.X., Atroshchenko, E., Nguyen-Xuan, H., Vo, T.P.: Geometrically nonlinear isogeometric analysis of functionally graded microplates with the modified couple stress theory. Comput. Struct. **193**, 110–127 (2017)
33. Sahmani, S., Fattahi, A.M.: Size-dependent nonlinear instability of shear deformable cylindrical nanopanels subjected to axial compression in thermal environments. Microsyst. Technol. **23**, 4717–4731 (2017)
34. Thai, S., Thai, H.-T., Vo, T.P., Nguyen-Xuan, H.: Nonlinear static and transient isogeometric analysis of functionally graded microplates based on the modified strain gradient theory. Eng. Struct. **153**, 598–612 (2017)
35. Sahmani, S., Aghdam, M.M.: Axial postbuckling analysis of multilayer functionally graded composite nanoplates reinforced with GPLs based on nonlocal strain gradient theory. Eur. Phys. J. Plus **132**, 490 (2017)
36. Liu, J.C., Zhang, Y.Q., Fan, L.F.: Nonlocal vibration and biaxial buckling of double-viscoelastic-FGM-nanoplate system with viscoelastic Pasternak medium in between. Phys. Lett. A **381**, 1228–1235 (2017)
37. Karami, B., Shahsavari, D., Li, L.: Hygrothermal wave propagation in viscoelastic graphene under in-plane magnetic field based on nonlocal strain gradient theory. Phys. E **97**, 317–327 (2018)
38. Sahmani, S., Fattahi, A.M.: Small scale effects on buckling and postbuckling behaviors of axially loaded FGM nanoshells based on nonlocal strain gradient elasticity theory. Appl. Math. Mech. **39**, 561–580 (2018)
39. Wang, Z., Xie, Z., Huang, W.: A pin-moment model of flexoelectric actuators. Int. J. Hydromech. **1**, 72–90 (2018)
40. Fang, J., Gu, J., Wang, H.: Size-dependent three-dimensional free vibration of rotating functionally graded microbeams based on a modified couple stress theory. Int. J. Mech. Sci. **136**, 188–199 (2018)
41. Sahmani, S., Aghdam, M.M.: Nonlinear instability of hydrostatic pressurized microtubules surrounded by cytoplasm of a living cell including nonlocality and strain gradient microsize dependency. Acta Mech. **229**, 403–420 (2018)
42. Rehab, I., Tian, X., Gu, F., et al.: The influence of rolling bearing clearances on diagnostic signatures based on a numerical simulation and experimental evaluation. Int. J. Hydromech. **1**, 16–46 (2018)
43. Thanh, C.-L., Phung-Van, P., Thai, C.H., Nguyen-Xuan, H., Wahab, A.: Isogeometric analysis of functionally graded carbon nanotube reinforced composite nanoplates using modified couple stress theory. Compos. Struct. **184**, 633–649 (2018)
44. Sahmani, S., Aghdam, M.M.: Nonlocal strain gradient shell model for axial buckling and postbuckling analysis of magneto-electro-elastic composite nanoshells. Compos. Part B Eng. **132**, 258–274 (2018)
45. Sahmani, S., Aghdam, M.M.: Nonlocal strain gradient beam model for postbuckling and associated vibrational response of lipid supramolecular protein micro/nano-tubules. Math. Biosci. **295**, 24–35 (2018)

46. Henderson, J.P., Plummer, A., Johnston, N.: An electro-hydrostatic actuator for hybrid active-passive vibration isolation. Int. J. Hydromech. **1**, 47–71 (2018)
47. Chu, L., Dui, G., Ju, C.: Flexoelectric effect on the bending and vibration responses of functionally graded piezoelectric nanobeams based on general modified strain gradient theory. Compos. Struct. **186**, 39–49 (2018)
48. Sahmani, S., Aghdam, M.M.: Thermo-electro-radial coupling nonlinear instability of piezoelectric shear deformable nanoshells via nonlocal elasticity theory. Microsyst. Technol. **24**, 1333–1346 (2018)
49. Zhang, K., Ge, M.-H., Zhao, C., Deng, Z.-C., Xu, X.-J.: Free vibration of nonlocal Timoshenko beams made of functionally graded materials by Symplectic method. Compos. Part B Eng. **156**, 174–184 (2019)
50. Sarafraz, A., Sahmani, S., Aghdam, M.M.: Nonlinear secondary resonance of nanobeams under subharmonic and superharmonic excitations including surface free energy effects. Appl. Math. Model. **66**, 195–226 (2019)
51. Lim, C.W., Zhang, G., Reddy, J.N.: A higher-order nonlocal elasticity and strain gradient theory and its applications in wave propagation. J. Mech. Phys. Solids **78**, 298–313 (2015)
52. Zhu, X., Li, L.: Twisting statics of functionally graded nanotubes using Eringen's nonlocal integral model. Compos. Struct. **178**, 87–96 (2017)
53. Zhu, X., Li, L.: On longitudinal dynamics of nanorods. Int. J. Eng. Sci. **120**, 129–145 (2017)
54. Tang, Y., Liu, Y., Zhao, D.: Wave dispersion in viscoelastic single walled carbon nanotubes based on the nonlocal strain gradient Timoshenko beam model. Phys. E **87**, 301–307 (2017)
55. Li, X., Li, L., Hu, Y., Ding, Z., Deng, W.: Bending, buckling and vibration of axially functionally graded beams based on nonlocal strain gradient theory. Compos. Struct. **165**, 250–265 (2017)
56. Ebrahimi, F., Dabbagh, A.: On flexural wave propagation responses of smart FG magneto-electro-elastic nanoplates via nonlocal strain gradient theory. Compos. Struct. **162**, 281–293 (2017)
57. Sahmani, S., Aghdam, M.M.: Size-dependent axial instability of microtubules surrounded by cytoplasm of a living cell based on nonlocal strain gradient elasticity theory. J. Theor. Biol. **422**, 59–71 (2017)
58. Lu, L., Guo, X., Zhao, J.: Size-dependent vibration analysis of nanobeams based on the nonlocal strain gradient theory. Int. J. Eng. Sci. **116**, 12–24 (2017)
59. Sahmani, S., Aghdam, M.M.: Nonlinear instability of axially loaded functionally graded multilayer graphene platelet-reinforced nanoshells based on nonlocal strain gradient elasticity theory. Int. J. Mech. Sci. **131–132**, 95–106 (2017)
60. Zhu, X., Li, L.: Closed form solution for a nonlocal strain gradient rod in tension. Int. J. Eng. Sci. **119**, 16–28 (2017)
61. Sahmani, S., Aghdam, M.M.: A nonlocal strain gradient hyperbolic shear deformable shell model for radial postbuckling analysis of functionally graded multilayer GPLRC nanoshells. Compos. Struct. **178**, 97–109 (2017)
62. Li, L., Hu, Y.: Post-buckling analysis of functionally graded nanobeams incorporating nonlocal stress and microstructure-dependent strain gradient effects. Int. J. Mech. Sci. **120**, 159–170 (2017)
63. Sahmani, S., Aghdam, M.M.: Nonlocal strain gradient beam model for nonlinear vibration of prebuckled and postbuckled multilayer functionally graded GPLRC nanobeams. Compos. Struct. **179**, 77–88 (2017)
64. Sahmani, S., Aghdam, M.M.: Nonlinear primary resonance of micro/nano-beams made of nanoporous biomaterials incorporating nonlocality and strain gradient size dependency. Results Phys. **8**, 879–892 (2018)
65. Radwan, A.F., Sobhy, M.: A nonlocal strain gradient model for dynamic deformation of orthotropic viscoelastic graphene sheets under time harmonic thermal load. Phys. B **538**, 74–84 (2018)
66. Sahmani, S., Aghdam, M.M., Rabczuk, T.: Nonlinear bending of functionally graded porous micro/nano-beams reinforced with graphene platelets based upon nonlocal strain gradient theory. Compos. Struct. **186**, 68–78 (2018)
67. Sahmani, S., Aghdam, M.M., Rabczuk, T.: A unified nonlocal strain gradient plate model for nonlinear axial instability of functionally graded porous micro/nano-plates reinforced with graphene platelets. Mater. Res. Expr. **5**, 045048 (2018)
68. Sahmani, S., Aghdam, M.M., Rabczuk, T.: Nonlocal strain gradient plate model for nonlinear large-amplitude vibrations of functionally graded porous micro/nano-plates reinforced with GPLs. Compos. Struct. **198**, 51–62 (2018)
69. Li, L., Tang, H., Hu, Y.: The effect of thickness on the mechanics of nanobeams. Int. J. Eng. Sci. **123**, 81–91 (2018)
70. Hedayati, R., Sadighi, M., Aghdam, M.M., Zadpoor, A.A.: Analytical relationships for the mechanical properties of additively manufactured porous biomaterials based on octahedral unit cells. Appl. Math. Model. **46**, 408–422 (2017)
71. Sun, J., Yang, Y., Wang, D.: Mechanical properties of Ti–6al–4V octahedral porous material unit formed by selective laser melting. Adv. Mech. Eng. Article ID: 427386 (2012)
72. Yang, L.: Experimental-assisted design development for an octahedral cellular structure using additive manufacturing. Rapid Prototyp. J. **21**, 168–176 (2015)
73. Hedayati, R., Sadighi, M., Aghdam, M.M., Zadpoor, A.A.: Effect of mass multiple counting on the elastic properties of open-cell regular porous biomaterials. Mater. Des. **89**, 9–20 (2016)
74. Rao, S.S.: Vibration of Continuous Systems. Wiley, New York (2007)